Inorg. Chem. **2007**, *46*, 9616–9629

On the Prospects of Polynuclear Complexes with Acetylenedithiolate Bridging Units

Wolfram W. Seidel,*,† Matthias J. Meel,† Udo Radius,‡ Markus Schaffrath,† and Tania Pape†

Institut für Anorganische und Analytische Chemie, Westfälische Wilhelms-Universität Münster, Corrensstrasse 30/36, D-48149 Münster, Germany, and Institut für Anorganische Chemie, Universität Karlsruhe (TH), Engesserstrasse, Geb. 30.45, D-76131 Karlsruhe, Germany

Received April 30, 2007

The generation of polynuclear complexes with one, two, or four acetylenedithiolate bridging units via the isolation of η^2-alkyne complexes of acetylenedithiolate K[Tp′M(CO)(L)(C_2S_2)] (Tp′ = hydrotris(3,5-dimethylpyrazolyl)borate, M = W, L = CO (K-**3a**), M = Mo, L = $CNC_6H_3Me_2$ (K-**3b**)) is reported. The strong electronic cooperation of Ru and W in the heterobimetallic complexes [(η^5-C_5H_5)(PPh_3)Ru(**3a**)] (**4a**) and [(η^5-C_5H_5)($Me_2C_6H_3NC$)Ru(**3a**)] (**4b**) has been elucidated by correlation of the NMR, IR, UV–vis, and EPR-spectroscopic properties of the redox couples **4a**/**4a**$^+$ and **4b**/**4b**$^+$ with results from density functional calculations. Treatment of M(II) (M = Ni, Pd, Pt) with K-**3a** and K-**3b** afforded the homoleptic bis complexes [M(**3a**)$_2$] (M = Ni (**5a**), Pd (**5b**), Pt (**5c**)), and [M(**3b**)$_2$] (M = Pd (**6a**) and Pt (**6b**)), in which the metalla-acetylendithiolates exclusively serve as S,S′-chelate ligands. The vibrational and electronic spectra as well as the cyclic voltammetry behavior of all the complexes are compared. The structural analogy of **5a**/**5b**/**5c** and **6a**/**6b** with dithiolene complexes is only partly reflected in the electronic structures. The very intense visible absorptions involve essential d orbital contributions of the central metal, while the redox activity is primarily attributed to the alkyne complex moiety. Accordingly, stoichiometric reduction of **5a**/**5b**/**5c** yields paramagnetic complex anions with electron-rich alkyne complex moieties being indistinguishable in the IR time scale. K-**3a** forms with Cu(I) the octanuclear cluster [Cu(**3a**)]$_4$ (**7**) exhibiting a $Cu_4(S_2C_2)_4W_4$ core. The nonchelating bridging mode of the metalla-acetylenedithiolate **3a**$^-$ in **7** is recognized by a high-field shift of the alkyne carbon atoms in the ^{13}C NMR spectrum. X-ray diffraction studies of K[Tp′(CO)(Me_3CNC)Mo(η^2-C_2S_2)] (K-**3c**), **4b**, **6a**, **6b**, and **7** are included. Comparison of the molecular structures of K-**3c** and **7** on the one hand with **4b** and **6a**/**6b** on the other reveals that the small bend-back angles in the latter are a direct consequence of the chelate ring formation.

Introduction

The coordination chemistry of small bridging ligands with π-conjugated donor centers has attracted increasing attention in the past decade due to the potential applications of resulting oligonuclear complexes or coordination polymers.[1] Functional materials with interesting magnetic[2] and electro-optical[3] properties in particular are frequently constructed by the assembly of mononuclear compounds and small bridging ligands to give polynuclear complexes with ligand-mediated metal−metal interaction. Although a variety of sulfur donor ligands such as tetrathiooxalate[4] and tetrathiosquarate[5] have been employed for this purpose, so far, less attention has been drawn to the four-atom acetylenedithiolate ligand. The dianion $(S-C\equiv C-S)^{2-}$ has the potential to support electronic communication between metal centers because each atom provides a coordination site for transition metals. Thus, the ambidentate nature as well as the flexibility in the electron donor capabilities of the acetylenedithiolate ligand promise a versatile coordination behavior. Considering the propensity of thiolate groups to bridge two metal ions and the capability of alkynes to coordinate two metal centers by the two π systems, acetylenedithiolate could potentially link up to six metal centers. Although first reports on metal complexes with alkyne-1-thiolates appeared in the past decade,[6] a decent development of the coordination chemistry of acetylenedithiolate is probably hampered by an intrinsic

* To whom correspondence should be addressed. E-mail: seidelww@uni-muenster.de.
† Westfälische Wilhelms-Universität Münster.
‡ Universität Karlsruhe.

10.1021/ic7008286 CCC: $37.00
Published on Web 10/18/2007

instability of acetylenedithiol[7] and, in addition, its corresponding base in the presence of any protic impurities.

Our approach to bypass this instability problem of the uncoordinated ligand lies in the usage of bis(benzylthio)-acetylene as a suitable precursor for acetylenedithiolate. The coordination of the alkyne entity of bis(benzylthio)acetylene to a metal center and subsequent reductive cleavage of the sulfur benzyl carbon bond affords suitable precursors for polynuclear complexes. The two-step, single-electron reduction[8] of $[Tp'(CO)_2W(\eta^2\text{-}BnSC_2SBn)](PF_6)$ {Tp′ = hydrotris-(3,5-dimethylpyrazolyl)borate} led to the alkyne complex $K[Tp'(CO)_2W(\eta^2\text{-}C_2S_2)]$ (K-**3a**), which can subsequently be reacted with a variety of metal precursors. Recently, we reported the first dinuclear and trinuclear heterobimetallic compounds featuring the hitherto unprecedented $\mu\text{-}\eta^2$-C,C′-k^2-S,S′ bridging mode of acetylenedithiolate.[9] Accordingly, alkyne complex formation renders acetylenedithiolate a dithiolate chelate ligand.

The structural similarity of the planar C_2S_2M-chelate rings in $[(\eta^5\text{-}C_5H_5)(PPh_3)Ru(\mathbf{3a})]$[9a] and $[M(\mathbf{3a})_2]$[9b] (M = Ni, Pd, Pt) with classical dithiolene complexes[10] has prompted us to perform detailed studies on the electronic properties of these complexes. First experiments on these compounds indicated the stability in two oxidation states and a strong coupling of the different metal atoms mediated by the C_2S_2 bridges. Considering $\mathbf{3a}^-$ as a metalla-acetylenedithiolate ligand, the donor/acceptor properties of the sulfur atoms might be easily adjusted by variation of the ancillary ligands in the alkyne complex moiety. Minor variations in the coordination sphere of the metalla-acetylenedithiolate ligand, as performed in this study, might act as a valuable diagnostic tool for the assignment of oxidation states, the elucidation of electronic transitions, or frontier orbital mixing.

In this contribution, we wish to report a careful study on tungsten-based polynuclear acetylenedithiolato complexes and the extension of our approach to molybdenum isocyanide-based systems, i.e., synthesis and characterization of $K[Tp'(CO)(2,6\text{-}Me_2C_6H_3NC)Mo(\eta^2\text{-}C_2S_2)]$ (K-**3b**) and $K[Tp'(CO)(t\text{-}BuNC)Mo(\eta^2\text{-}C_2S_2)]$ (K-**3c**). Furthermore, we report the X-ray crystal structure of K-**3c**, which is the first structural report of an acetylenedithiolate complex featuring two terminal sulfur atoms. In addition, the synthesis and full characterization of the dinuclear complexes $[(\eta^5\text{-}C_5H_5)(L)Ru(\mathbf{3a})]$ (L = PPh_3, $CNC_6H_3Me_2$) and of the trinuclear complexes $[M(\mathbf{3a})_2]$ (M = Ni, Pd, Pt) and $[M(\mathbf{3b})_2]$ (M = Pd, Pt) are described. All these compounds turned out to be stable in two oxidation states. The detailed investigation of the spectroscopic parameters of these closely related complexes, including cyclic voltammetry and electron paramagnetic resonance (EPR) spectroscopy data, allows one to draw conclusions on their electronic structure, which are supported by density functional theory (DFT) calculations on the dinuclear complexes $[(\eta^5\text{-}C_5H_5)(L)Ru(\mathbf{3a})]$. The question of the general coordination behavior of metalla-acetylenedithiolate ligands will be addressed by experiments with the d^{10} metal center Cu(I).

Experimental Section

All operations were carried out under a dry argon atmosphere using standard Schlenk and glovebox techniques. All solvents were dried and saturated with argon by standard methods and freshly distilled prior to use. $[Tp'W(CO)_2(BnSC_2S)]$ (**2a**), $[Tp'Mo(CO)(2,6\text{-}Me_2C_6H_3NC)(BnSC_2S)]$ (**2b**), and $[Tp'Mo(CO)(Me_3CNC)(BnSC_2S)]$ (**2c**) were prepared according to published procedures.[8,11] $[(C_5H_5)Ru(CH_3CN)_2(PPh_3)](PF_6)$,[12] $[(C_5H_5)Ru(CH_3CN)_2(2,6\text{-}Me_2C_6H_3NC)](PF_6)$,[12] and $[Ni(CH_3CN)_6](BF_4)_2$[13] were obtained by literature methods. NMR spectra were recorded on Bruker AC 200

(1) (a) Chandrasekhar, V. *Inorganic and Organometallic Polymers*; Springer-Verlag: Berlin, 2005. (b) Archer, R. D. *Inorganic and Organometallic Polymers*; Wiley-VCH: Weinheim, Germany, 2001. (c) Manners, I. *Synthetic Metal-Containing Polymers*; Wiley-VCH: Weinheim, Germany, 2004.

(2) (a) Balzani, V.; Campagna, S.; Denti, G.; Alberto, J.; Serroni, S.; Venturi, M. *Acc. Chem. Res.* **1998**, *31*, 26−34. (b) Paw, W.; Cummings, S. D.; Mansour, M. A.; Connick, W. B.; Geiger, D. K.; Eisenberg, R. *Coord. Chem. Rev.* **1998**, *171*, 125−150. (c) Barigelletti, F.; Flamigni, L. *Chem. Soc. Rev.* **2000**, *29*, 1−12. (d) Grätzel, M. *Inorg. Chem.* **2005**, *44*, 6841−6851. (e) Meyer, G. J. *Inorg. Chem.* **2005**, *44*, 6852−6864. (f) Jukes, R. T. F.; Adamo, V.; Hartl, F.; Belser, P.; De Cola, L. *Coord. Chem. Rev.* **2005**, *249*, 1327−1335. (g) Gagliardo, M.; Rodriguez, G.; Dam, H. H.; Lutz, M.; Spek, A. L.; Havenith, R. W. A.; Coppo, P.; De Cola, L.; Hartl, F.; van Klink, G. P. M.; van Koten, G. *Inorg. Chem.* **2006**, *45*, 2143−2155. (h) Maji, S.; Sarkar, B.; Patra, S.; Fiedler, J.; Mobin, S.; Puranik, V. G.; Kaim, W.; Lahiri, G. K. *Inorg. Chem.* **2006**, *45*, 1316−1325.

(3) (a) Ferlay, S.; Mallah, T.; Ouahes, R.; Veillet, P.; Verdaguer, M. *Nature* **1995**, *378*, 701−703. (b) Kahn, O. *Acc. Chem. Res.* **2000**, *33*, 647−657. (c) Miller, J. S.; Manson, J. L. *Acc. Chem. Res.* **2001**, *34*, 563−570. (d) Gatteschi, D.; Sessoli, R. *J. Magn. Magn. Mater.* **2004**, *272−276*, 1030−1036. (e) Beltran, L. M. C.; Long, J. R. *Acc. Chem. Res.* **2005**, *38*, 325−334. (f) Glaser, T.; Heidemeier, M.; Weyermüller, T.; Hoffmann, R.-D.; Rupp, H.; Müller, P. *Angew. Chem.* **2006**, *118*, 6179−6183.

(4) (a) Yang, X.; Doxsee, D. D.; Rauchfuss, T. B.; Wilson, S. R. *J. Chem. Soc., Chem. Commun.* **1994**, 821−822. (b) Pullen, A. E.; Zeltner, S.; Olk, R.-M.; Hoyer, E.; Abboud, K. A.; Reynolds, J. R. *Inorg. Chem.* **1997**, *36*, 4163−4171. (c) Holloway, G.; Klausmeyer, K. K.; Wilson, S. R.; Rauchfuss, T. B. *Organometallics* **2000**, *19*, 5370−5375. (d) Pyrasch, M.; Amirbeyki, D.; Tieke, B. *Adv. Mater.* **2001**, *13*, 1188−1191. (e) Guyon, F.; Jourdain, I. V.; Knorr, M.; Lucas, D.; Monzon, T.; Mugnier, Y.; Avarvari, N.; Fourmigue, M. *Eur. J. Inorg. Chem.* **2002**, 2026−2033. (f) Kubo, K.; Nakao, A.; Yamamoto, H. M.; Kato, R. *J. Am. Chem. Soc.* **2006**, *128*, 12358−12359.

(5) Grenz, R.; Goetzfried, F.; Nagel, U.; Beck, W. *Chem. Ber.* **1986**, *119*, 1217−1231.

(6) (a) Weigand, W. *Z. Naturforsch.* **1991**, *46b*, 1333−1337. (b) Weigand, W.; Weishäupl, M.; Robl, C. *Z. Naturforsch.* **1996**, *51b*, 501−505. (c) Sugiyama, H.; Hayashi, Y.; Kawaguchi, H.; Tatsumi, K. *Inorg. Chem.* **1998**, *37*, 6773−6779. (d) Sunada, Y.; Hayashi, Y.; Kawaguchi, H.; Tatsumi, K., *Inorg. Chem.* **2001**, *40*, 7072−7078. (e) Ara, I.; Delgado, E.; Fornies, J.; Hernandes, E.; Lalinde, E.; Mansilla, N.; Moreno, M. T. *J. Chem. Soc., Dalton Trans.* **1998**, 3199−3208. (f) Alcalde, M. I.; Carty, A. J.; Chi, Y.; Delgado, E.; Donnadieu, B.; Hernandez, E.; Dallmann, K.; Sanches-Nieves, J. *J. Chem. Soc., Dalton Trans.* **2001**, 2502−2507.

(7) (a) Diehl, F.; Meyer, H.; Schweig, A.; Hess, B. A., Jr.; Fabian, J. *J. Am. Chem. Soc.* **1989**, *111*, 7651−7653. (b) Timoshkin, A.; Frenking, G. *J. Chem. Phys.* **2000**, *113*, 8430−8433. (c) Vijay, D.; Sastry, G. N. *THEOCHEM* **2005**, *732*, 71−78.

(8) Seidel, W. W.; Ibarra Arias, M. D.; Schaffrath, M.; Jahnke, M.; Hepp, A.; Pape, T. *Inorg. Chem.* **2006**, *45*, 4791−4800.

(9) (a) Seidel, W. W.; Schaffrath, M.; Pape, T. *Angew. Chem.* **2005**, *44*, 7798−7800. (b) Seidel, W. W.; Schaffrath, M.; Pape, T. *Chem. Commun.* **2006**, 3999−4000.

(10) Beswick, C. L.; Schulman, J. M.; Stiefel, E. I. *Prog. Inorg. Chem.* **2004**, *52*, 55−110.

(11) Seidel, W. W.; Lopez Sanchez, B.; Meel, M.; Hepp, A.; Pape, T. *Eur. J. Inorg. Chem.* **2007**, 936−943.

(12) Rüba, E.; Simanko, W.; Mauthner, K.; Soldouzi, K. M.; Slugovc, C.; Mereiter, K.; Schmid, O.; Kirchner, K. *Organometallics* **1999**, *18*, 3843−3850.

(13) Heintz, R. A.; Smith, J. A.; Szalay, P. S.; Weisgerber, A.; Dunbar, K. R. *Inorg. Synth.* **2002**, *33*, 75−83.

Table 1. Crystallographic Data for K-**3c**·THF, **4b**, **6a**·4Toluene, **6b**·4Toluene, and **7**·3Toluene

	K-**3c**·THF	**4b**	**6a**·4Toluene	**6b**·4Toluene	**7**·3Toluene
chemical formula	$C_{27}H_{39}BKMoN_7O_2S_2$	$C_{33}H_{36}BN_7O_2RuS_2W$	$C_{82}H_{94}B_2Mo_2N_{14}O_2PdS_4$	$C_{82}H_{94}B_2Mo_2N_{14}O_2PtS_4$	$C_{97}H_{112}B_4Cu_4N_{24}O_8S_8W_4$
fw	703.62	922.54	1755.85	1844.54	3031.39
space group	$I\bar{4}$	$P\bar{1}$	$P\bar{1}$	$P\bar{1}$	$P\bar{1}$
a (Å)	28.9380(5)	10.8601(13)	11.2667(17)	11.2664(15)	15.751(4)
b (Å)	28.9380(5)	11.1179(13)	13.802(2)	13.7944(18)	20.272(5)
c (Å)	8.2392(2)	16.4084(18)	14.509(2)	14.5269(19)	20.290(5)
α (deg)	90	85.038(3)	98.510(3)	98.657(3)	91.679(6)
β (deg)	90	81.826(3)	99.285(3)	99.151(3)	110.126(5)
γ (deg)	90	63.096(2)	108.812(3)	108.727(2)	98.225(6)
V (Å^3)	6899.6(2)	1748.2(3)	2058.9(5)	2061.3(5)	5999(3)
Z	8	2	1	1	2
T (K)	100	153	153	153	153
ρ_{calcd} (g cm^{-3})	1.355	1.753	1.416	1.486	1.678
reflns collcd/$2\Theta_{max}$	20133/140.14	20710/60.14	20269/55.0	23776/60.04	49010/50.0
unique reflns/$I > 2\sigma(I)$	5826/4594	10124/7380	9427/7100	11794/9843	21136/14758
no. of params/restr	350/0	432/0	514/6	494/0	1351/14
μ (mm^{-1})/λ (Å)	5.595/1.54178	3.880/0.71073	0.672/0.71073	2.148/0.71073	4.711/0.71073
R1[a]/GOF[b]	0.0499/0.965	0.0494/0.962	0.0432/1.018	0.0429/1.037	0.0512/1.006
wR2[c] ($I > 2\sigma(I)$)	0.1188	0.0928	0.1007	0.1020	0.1185
resid density (e·Å^{-3})	+1.036/−0.556	+2.393/−1.098	+0.821/−0.488	+2.18/−1.174	+2.736/−1.376

[a] Observation criterion: $I > 2\sigma(I)$. R1 = $\sum||F_o| - |F_c||/\sum|F_o|$. [b] GOF = $[\sum[w(F_o^2 - F_c^2)^2]/(n-p)]^{1/2}$. [c] wR2 = $[\sum[w(F_o^2 - F_c^2)^2]/\sum w(F_o^2)^2]]^{1/2}$, where $w = 1/\sigma^2(F_o^2) + (aP)^2 + bP$, $P = (F_o^2 + 2F_c^2)/3$.

and Bruker Avance 400 NMR spectrometers. X-band EPR spectra were recorded on a Bruker ELEXSYS E500 spectrometer equipped with a helium flow cryostat (Oxford Instruments ESR 910) and a Hewlett-Packard frequency counter HP5253B. EPR simulations were performed with the program *EPR* written by F. Neese, MPI for Bioinorganic Chemistry, Mülheim. Elemental analyses were performed on a Vario EL III CHNS elemental analyzer. Electrospray ionization (ESI) mass spectra were obtained using a QUATTRO LCZ (Waters-Micromass). Infrared spectra were recorded on a Bruker Vektor 22. Electronic spectra were obtained on Varian CARY 50 and on CARY 5000 spectrometers. Cyclic voltammetry data were acquired on a ECO/Metrohm PGSTAT 30 potentiostat using a glassy-carbon working electrode, a Ag/0.01 M $AgNO_3$/CH_3CN reference electrode, $(NBu_4)(PF_6)$ as supporting electrolyte, and ferrocene as internal standard.

K[Tp′W(CO)$_2$(η^2-SC$_2$S)] (K-3a). At −78 °C, potassium graphite (C_8K, 68 mg, 0.5 mmol) was added to a solution of green **2a** (300 mg, 0.42 mmol) in tetrahydrofuran (THF, 10 mL) leading to an intensely purple solution. The solution turned brown upon warming to ambient temperature. After 12 h of stirring, the solution was filtered through a pad of celite and the solvent was removed in vacuo. The residue was dissolved in a minimum of THF and layered with *n*-hexane (20 mL). The brown precipitate formed overnight was isolated and dried in vacuo. K-**3a** was sufficiently pure for further experiments. Yield: 134 mg (48%). IR (KBr, cm^{-1}): ν 1976 (s, CO), 1896 (s, CO), 1624 (w, SC−CS). ^{1}H NMR (THF-d_8, 30 °C): δ 5.92 (s, 1 H, C*H*(CCH$_3$)$_2$), 5.77 (s, 2 H, C*H*(CCH$_3$)$_2$), 4.40−4.90 (s, br, 1 H, B*H*), 2.57 (s, 3 H, CC*H*$_3$), 2.43 (s, 6 H, CC*H*$_3$), 2.34 (s, 3 H, CC*H*$_3$), 1.68 (s, 6 H, CC*H*$_3$). ^{13}C{^{1}H} NMR (THF-d_8, −60 °C): δ 290.8 (W*C*S), 251.9 (W*C*S), 224.6 (W*C*O), 153.4, 151.1, 145.9, 143.1 (CH(*C*CH$_3$)$_2$), 107.3, 106.2 (*C*H-(CCH$_3$)$_2$), 15.7, 15.3, 14.4, 12.2 (C*C*H$_3$).

K[Tp′Mo(CO)(2,6-Me$_2$C$_6$H$_3$NC)(η^2-SC$_2$S)] (K-3b). K-**3b** was synthesized analogously to K-**3a** using **2b** (400 mg, 0.55 mmol) in THF (10 mL). Reduction of dark yellow **2b** at −78 °C caused a color change to intense moss-green and finally to brown upon warming. Yield: 198 mg (53%). IR (KBr, cm^{-1}): ν 2050 (s, C≡N), 1917 (s, CO), 1590 (w, SC−CS). ^{1}H NMR (CD_3CN, 30 °C): δ 7.50−6.80 (m, 3 H, C$_6$*H*$_3$Me$_2$), 5.93 (s, 1 H, C*H*(CCH$_3$)$_2$), 5.83 (s, 1 H, C*H*(CCH$_3$)$_2$), 5.67 (s, 1 H, C*H*(CCH$_3$)$_2$), 4.68 (s, br, 1 H, B*H*), 2.54 (s, 3 H, CC*H*$_3$), 2.53 (s, 3 H, CC*H*$_3$), 2.44 (s, 3 H, CC*H*$_3$), 2.38 (s, 3 H, CC*H*$_3$), 2.37 (s, 6 H, C$_6$H$_3$(C*H*$_3$)$_2$), 2.00 (s, 3 H, CC*H*$_3$), 1.38 (s, 3 H, CC*H*$_3$). ^{13}C{^{1}H} NMR (CD_3CN, 30 °C): δ 297.5, 273.7 (Mo*C*S), 237.1 (Mo*C*O), 189.0 (Mo*C*N), 154.1, 152.9, 151.7, 147.1, 144.9, 144.8 (CH(*C*CH$_3$)$_2$), 134.7 (*o*-C$_6$H$_3$Me$_2$), 128.9, 128.8, 128.7 (C$_6$H$_3$Me$_2$), 108.0, 107.6, 107.1 (*C*H(CCH$_3$)$_2$), 19.7 (C$_6$H$_3$*C*H$_3$), 15.7, 15.6, 14.5, 13.2, 13.1, 13.0 (C*C*H$_3$).

K[Tp′Mo(CO)(Me$_3$CNC)(η^2-SC$_2$S)] (K-3c). K-**3c** was synthesized analogously to K-**3a** using **2c** (310 mg, 0.45 mmol) in THF (30 mL). Reduction of green **2c** at −78 °C caused a color change to intensely red. The residue, after filtration and evaporation of THF, was dissolved in toluene (1 mL) and THF (2 mL). Evaporation of THF led to the crystallization of analytically pure K-**3c**. Yield: 195 mg (68%). Anal. Calcd for K-**3c**·THF, $C_{27}H_{39}BKMoN_7O_2S_2$: C, 46.09; H, 5.59; N, 13.93; S, 9.11. Found: C, 45.85; H, 5.36; N, 13.90; S, 8.96. IR (KBr, cm^{-1}): ν 2121 (s, C≡N), 1906 (s, CO). ^{1}H NMR (CD_3CN, 30 °C): δ 5.87 (s, 1 H, C*H*(CCH$_3$)$_2$), 5.84 (s, 1 H, C*H*(CCH$_3$)$_2$), 5.66 (s, 1 H, C*H*(CCH$_3$)$_2$), 2.64 (s, 3 H, CC*H*$_3$), 2.50 (s, 3 H, CC*H*$_3$), 2.43 (s, 3 H, CC*H*$_3$), 2.36 (s, 3 H, CC*H*$_3$), 1.85 (s, 3 H, CC*H*$_3$), 1.42 (s, 9 H, C(C*H*$_3$)$_3$), 1.33 (s, 3 H, CC*H*$_3$). ^{13}C{^{1}H} NMR (CD_3CN, 30 °C): δ 293.6, 269.8 (Mo*C*S), 239.3 (Mo*C*O), 170.8 (Mo*C*N), 154.1, 152.7, 151.3, 147.1, 144.9, 144.8 (*C*CH$_3$), 107.8, 107.5, 107.0 (*C*H(CCH$_3$)$_2$), 58.1 (*C*(CH3)$_3$), 31.3 (C(*C*H$_3$)$_3$), 15.7, 15.3, 14.6, 13.1, 13.0, 13.0 (C*C*H$_3$).

[Tp′(CO)$_2$W(μ-η^2-η^2-C$_2$S$_2$)Ru(η^5-C$_5$H$_5$)(PPh$_3$)] (4a). [(η^5-C_5H_5)Ru(PPh$_3$)(CH$_3$CN)$_2$](PF$_6$) (151 mg, 0.23 mmol) was added to a solution of 153 mg (0.23 mmol) K-**3a** in 20 mL of THF. The solution turned blue and was stirred for 12 h. The solvent was evaporated in vacuo and the residue was dissolved in a minimum amount of toluene and purified by column chromatography on SiO_2 using toluene as eluent. Crystallization was achieved by gas-phase diffusion of *n*-hexane into a THF solution of **4a**. Yield: 60 mg (25%). Anal. Calcd for $C_{42}H_{42}BN_6O_2PRuS_2W$: C, 47.88; H, 4.02; N, 7.98; S, 6.09. Found: C, 47.85; H, 4.19; N, 7.85; S, 6.02. IR (KBr, cm^{-1}): ν 1980 (s, CO), 1904 (s, CO). ^{1}H NMR ($CDCl_3$, −60 °C): δ 7.36 (m, 6 H, PC$_6$*H*$_5$), 7.29 (m, 9 H, PC$_6$*H*$_5$), 5.85 (s, 1 H, C*H*(CCH$_3$)$_2$), 5.83 (s, 1 H, C*H*(CCH$_3$)$_2$), 5.77 (s, 1 H, C*H*(CCH$_3$)$_2$), 4.17 (s, 5 H, C$_5$*H*$_5$), 2.44 (s, 3 H, CC*H*$_3$), 2.33 (s, 3 H, CC*H*$_3$), 2.32 (s, 3 H, CC*H*$_3$), 2.27 (s, 3 H, CC*H*$_3$), 2.16 (s, 3 H, CC*H*$_3$), 1.94 (s, 3 H, CC*H*$_3$). ^{13}C{^{1}H} NMR ($CDCl_3$, −60 °C): δ

278.1, 259.3 (W*C*S), 224.9, 219.3 (W*C*O), 153.4, 153.2, 152.2, 145.7, 144.2, 143.9 (CH(*C*CH_3)$_2$), 136.2 (d, 9 Hz), 133.6 (d, 19 Hz), 128.5 (d, 7 Hz), 127.5 (d, 9 Hz, P*C*$_6H_5$), 107.8, 106.9, 106.9 (*C*H(*C*CH_3)$_2$), 77.6 (*C*$_5H_5$), 15.9, 15.6, 15.5, 13.1, 13.0, 12.9 (C*C*H_3). $^{31}P\{^1H\}$ NMR ($CDCl_3$, 30 °C): δ 55.9.

[Tp′(CO)$_2$W(μ-η^2-η^2-C_2S_2)Ru(η^5-C_5H_5)($CNC_6H_3Me_2$)] (4b). 4b was synthesized analogously to **4a** using K-**3a** (121 mg, 0.18 mmol) and [(η^5-C_5H_5)Ru($CNC_6H_3Me_2$)(CH_3CN)$_2$](PF_6) (95 mg, 0.18 mmol) in THF (20 mL) leading to a purple solution. Yield after chromatography and crystallization: 55 mg (33%). Anal. Calcd for $C_{33}H_{36}BN_7O_2RuS_2W$: C, 42.96; H, 3.93; N, 10.63; S, 6.95. Found: C, 43.07; H, 4.05; N, 10.53; S, 6.92. IR (KBr, cm^{-1}): ν 2053 (s, C≡N), 1969 (s, CO), 1905 (s, CO). ^1H NMR ($CDCl_3$, −60 °C): δ 7.30 (t, 1 H, $C_6H_3Me_2$), 7.21 (d, 2 H, $C_6H_3Me_2$), 5.95 (s, 1 H, C*H*(CCH_3)$_2$), 5.88 (s, 1 H, C*H*(CCH_3)$_2$), 5.80 (s, 1 H, C*H*(CCH_3)$_2$), 4.75 (s, 5 H, C_5H_5), 2.60 (s, 3 H, CC*H*$_3$), 2.49 (s, 3 H, CC*H*$_3$), 2.34 (s, 6 H, $CNC_6H_3(CH_3)_2$), 2.30 (s, 3 H, CC*H*$_3$), 2.29 (s, 6 H, CC*H*$_3$), 1.95 (s, 3 H, CC*H*$_3$). $^{13}C\{^1H\}$ NMR ($CDCl_3$, −60 °C): δ 277.7, 260.7 (W*C*S), 221.5, 218.4 (W*C*O), 173.1 (*C*$NC_6H_3Me_2$), 153.5, 153.2, 152.6, 146.1, 144.3, 144.2 (CH(*C*CH_3)$_2$), 133.5 (*o*-$C_6H_3Me_2$), 130.5, 127.2, 125.4 ($C_6H_3Me_2$), 108.0, 107.3, 107.2 (*C*H(*C*CH_3)$_2$), 78.9 (*C*$_5H_5$), 19.4 ($CNC_6H_3(CH_3)_2$), 16.0, 15.6, 15.0, 13.1, 13.0, 12.9 (C*C*H_3).

Oxidation of 4a/b. A solution of **4a** (105 mg, 0.1 mmol) in CH_2Cl_2 (20 mL) was treated with solid $AgBF_4$ (20 mg, 0.1 mmol). After 30 min, the purple solution was filtered. ESI MS (CH_2Cl_2): *m*/*z* 1054 [**4a**$^+$], correct isotopic pattern, 764 [**4a**$^+$ − PPh_3 − CO], 736 [**4a**$^+$ − PPh_3 −2CO]. A CH_2Cl_2 solution of [**4b**-BF_4] was obtained accordingly. A crystalline sample of [**4a**-PF_6] in form of purple needles was obtained after oxidation of **4a** with [(η^5-C_5H_5)$_2$Fe](PF_6) and subsequent gas-phase diffusion of Et_2O into the CH_2Cl_2 solution.

[{Tp′(CO)$_2$W(μ-η^2-η^2-C_2S_2)}$_2$Ni] (5a). Synthesis of **5a** is given as a standard procedure, which applies also to **5b**/**5c** and **6a**/**6b**. A solution of [Ni(CH_3CN)$_6$](BF_4)$_2$ (80 mg, 0.167 mmol) in CH_2Cl_2 (20 mL) was added to a stirred solution of K-**3a** (222 mg, 0.334 mmol) in THF (15 mL). The color of the solution turned blue immediately. After 5 h, the solvents were removed in vacuo. The residue was dissolved in a minimum amount of THF and transferred on a chromatography column containing SiO_2 and toluene. The product **5a** was eluted with a toluene/THF mixture (v/v: 5/1) and crystallized from the eluated solution without any volume reduction in the course of two weeks. Yield: 27 mg (11%). Anal. Calcd for **5a**·2 toluene, $C_{52}H_{60}B_2N_{12}NiO_4S_4W_2$: C, 41.82; H, 4.05; N, 11.25. Found: C, 41.68; H, 3.98; N, 11.14. ^1H NMR (CD_2Cl_2, 30 °C): δ 5.93 (s, 1 H, C*H*(CCH_3)$_2$), 5.92 (s, 2 H, C*H*(CCH_3)$_2$), 2.49 (s, 3 H, CC*H*$_3$), 2.40 (s, 6 H; CC*H*$_3$), 2.34 (s, 3 H, CC*H*$_3$), 2.31 (s, 6 H, CC*H*$_3$). IR (KBr, cm^{-1}): ν 2008, 1957 (s, CO).

[{Tp′(CO)$_2$W(μ-η^2-η^2-C_2S_2)}$_2$Pd] (5b). A solution of [Pd(CH_3CN)$_4$](BF_4)$_2$ (70 mg, 0.158 mmol) in CH_3CN (10 mL) was added to a stirred solution of K-**3a** (210 mg, 0.316 mmol) in THF (15 mL). The color of the solution immediately turned intensely red. Yield: 24 mg (10%). Anal. Calcd. for **5b**·2 toluene, $C_{52}H_{60}B_2N_{12}O_4PdS_4W_2$: C, 40.53; H, 3.92; N, 10.91. Found: C, 40.61; H, 3.95; N, 10.84. IR (KBr, cm^{-1}): ν 2010, 1959 (s, CO). A second dark-red fraction was eluated with THF. IR (THF, cm^{-1}): ν 2011, 1940 (s, CO). UV−vis (THF) λ_{max} = 451 nm. MALDI MS (CH_3CN, pos): *m*/*z* = 2795.8 [Pd_2(**3a**)$_4$(CH_3CN)$_2$], 2165.5 [Pd_2(**3a**)$_3$(CH_3CN)(H_2O)$_2$].

[{Tp′(CO)$_2$W(μ-η^2-η^2-C_2S_2)}$_2$Pt] (5c). A solution of [$PtCl_2$(NCPh)$_2$] (30 mg, 0.064 mmol) in CH_2Cl_2 (10 mL) was added to a stirred solution of K-**3a** (84 mg, 0.127 mmol) in THF (10 mL). The color of the solution turned intensely blue in the course of 16 h. Yield: 20 mg (19%). Anal. Calcd for **5c**·2 toluene, $C_{52}H_{60}B_2N_{12}O_4PtS_4W_2$: C, 38.32; H, 3.71; N, 10.31. Found: C, 38.33; H, 3.75; N, 10.21. IR (KBr, cm^{-1}): ν 2009, 1956 cm^{-1} (s, CO).

Reduction of 5a/5b/5c. A solution of $NaC_{10}H_8$ in THF (0.01 mol L^{-1}, 2 mL) was added to a solution of **5a** (26 mg), **5b** (27 mg), or **5c** (29 mg), 0.02 mmol, respectively, in THF (8 mL) inside a glovebox. The solutions turned yellow immediately. They were diluted and used for IR, UV−vis, and EPR spectroscopy.

[{Tp′(CO)(CNC_6H_3-2,6-Me_2)Mo(μ-η^2-η^2-C_2S_2)}$_2$Pd] (6a). 6a was synthesized analogously to **5b** using K-**3b** (150 mg, 0.22 mmol) in THF (20 mL) and [Pd(CH_3CN)$_4$](BF_4)$_2$ (49 mg, 0.11 mmol) in CH_3CN (20 mL). Yield after chromatography and crystallization: 33 mg (17%). Anal. Calcd. for **6a**·4 toluene, $C_{82}H_{94}B_2Mo_2N_{14}O_2PdS_4$: C, 56.09; H, 5.40; N, 11.17. Found: C, 55.92; H, 5.25; N, 11.24. ^1H NMR (CD_2Cl_2, 30 °C): δ 7.16−7.02 (m, $C_6H_3Me_2$, 6 H), 5.96 (s, 2 H, C*H*(CCH_3)$_2$), 5.85 (s, 2 H, C*H*(CCH_3)$_2$), 5.80 (s, 2 H, C*H*(CCH_3)$_2$), 2.61 (s, 6 H, CC*H*$_3$), 2.45 (s, 6 H, CC*H*$_3$), 2.43 (s, 6 H, CC*H*$_3$), 2.42 (s, 6 H, CC*H*$_3$), 2.39 (s, 12 H, $C_6H_3(CH_3)_2$), 2.36 (s, 6 H, CC*H*$_3$), 2.06 (s, 6 H, CC*H*$_3$).

[{Tp′(CO)(CNC_6H_3-2,6-Me_2)Mo(μ-η^2-η^2-C_2S_2)}$_2$Pt] (6b). 6b was synthesized analogously to **5c** using K-**3b** (150 mg, 0.22 mmol) in THF (20 mL) and [Pt(NCPh)$_2$Cl$_2$] (52 mg, 0.11 mmol) in CH_2Cl_2 (20 mL). Yield after chromatography and crystallization: 39 mg (19%). Anal. Calcd. for **6b**·4 toluene, $C_{82}H_{94}B_2Mo_2N_{14}O_2PtS_4$: C, 53.39; H, 5.14; N, 10.63. Found: C, 53.33; H, 5.10; N, 10.71. ^{195}Pt NMR (CD_2Cl_2, 30 °C): δ −2767.

[{Tp′(CO)$_2$Wμ-η^2-η^2-C_2S_2)}Cu]$_4$ (7). To a stirred solution of [Cu(CH_3CN)$_4$](BF_4) (44 mg, 0.14 mmol) in CH_2Cl_2 (20 mL) was added a solution of K-**3a** (93 mg, 0.14 mmol) in THF (10 mL). After stirring for 16 h, the intensely red solution was reduced to dryness. The residue was dissolved in a minimum of THF and subjected to chromatography (SiO_2, toluene). After separation of a yellow byproduct with toluene, product **7** was eluted with toluene/THF (v/v: 4/1). After removal of the solvents in vacuo, **7** was washed with *n*-hexane and dried in vacuo. Crystallization was achieved over the course of weeks from a toluene solution **7** with a minimum of THF obtained by reducing the volume of a toluene/THF solution. Yield after crystallization: 21 mg (23%). Anal. Calcd for **7**·3 toluene, $C_{97}H_{112}B_4Cu_4N_{24}O_8S_8W_4$: C, 38.43; H, 3.72; N, 11.09; S, 8.46. Found: C, 38.63; H, 3.81; N, 10.96; S, 8.36. IR (CH_2Cl_2, cm^{-1}): ν 2006 (m, CO), 1930 (s, CO).

Crystal Structure Determination. Single crystals suitable for X-ray diffraction were coated in paratone oil and mounted on a glass fiber. The intensity data of the complexes was collected on a Bruker AXS Apex system equipped with a rotating anode. The data was measured using either graphite-monochromated Mo Kα radiation (**4b**, **6a**, **6b**, **7**) or Goebel-mirror monochromated Cu Kα radiation (K-**3c**). Data collection, cell refinement, data reduction and integration, as well as absorption correction were performed with the Bruker AXS program packages *SMART*, *SAINT*, and *SADABS*. Crystal and space group symmetries were determined using the *XPREP* program. All crystal structures were solved with *SHELXS*[14] by direct methods and were refined by full-matrix least-square techniques against F_o^2 with *SHELXL*.[15] All non-hydrogen atoms were refined anisotropically. The hydrogen atoms were included at calculated positions with fixed displacement parameters. The details of the structure analyses are listed in Table 1.

Computational Details. All calculations were carried out with

(14) *SHELXS-97*: Sheldrick, G. M. *Acta Crystallogr., Sect A* **1990**, *46*, 467−473.
(15) *SHELXL-97*: Sheldrick, G. M.; Universität Göttingen: Göttingen, Germany, **1997**.

Table 2. Selected ^{13}C NMR and IR Spectroscopic Data

	^{13}C NMR (δ, ppm)			IR (ν, cm^{-1})	
complex	MCS	MCO	MCNR	MC≡O	MC≡NR
K−**3a** (M = W)	290.8, 251.9[a]	224.6[a]		1969, 1887[e]	
K−**3b** (M = Mo)	297.5, 273.1[b]	237.1[b]	189.0[b]	1917[f]	2050[f]
K−**3c** (M = Mo)	293.6, 269.8[b]	239.3[b]	170.8[b]	1906[f]	2121[f]
4a (M = W)	278.1, 259.3[c]	224.9, 219.3[c]		1984, 1910[g]	
4a-BF_4				2035, 1967[g]	
4b (M = W)	277.7, 260.7[c]	221.5, 218.4[c]		1988, 1918[g]	2056[g]
4b-BF_4				2038, 1970[g]	2143[g]
[Ni(**3a**)$_2$] (**5a**)		216.3[d]		2009, 1942[e]	
Na-**5a**				1974, 1894[e]	
[Pd(**3a**)$_2$] (**5b**)		216.2[d]		2008, 1940[e]	
Na-**5b**				1973, 1892[e]	
[Pt(**3a**)$_2$] (**5c**)		215.7[d]		2004, 1939[e]	
Na-**5c**				1994, 1925[e]	
[Pd(**3b**)$_2$] (**6a**)	272.3[d]	226.0[d]	175.8	1940[f]	2113[f]
[Pt(**3b**)$_2$] (**6b**)	268.2[d]	225.7[d]	175.3	1934[f]	2122[f]
[Cu(**3a**)]$_4$ (**7**)	256.6, 230.1[d]	221.0, 220.6[d]		2007, 1937[f]	

[a] THF-d_8, −60 °C. [b] CD_3CN, 30 °C. [c] $CDCl_3$, −60 °C. [d] CD_2Cl_2, 30 °C. [e] In THF. [f] In KBr. [g] In CH_2Cl_2.

the DFT implementation of the *TURBOMOLE* program package.[16] The DFT calculations were performed using the BP86 functional,[17] SV(P) basis sets, and the RI-J approximation.[18−20] Cartesian coordinates for geometry-optimized structures are listed in the Supporting Information. Analytic second derivatives were calculated with the module *AOFORCE*[21] using the RI-J approximation. The time-dependent (TDDFT) calculations for the excitation energies were performed with the *ESCF* program.[22]

Results and Discussion

Synthesis and Characterization of the Metalla-Acetylenedithiolate Ligands. According to the preparative procedure outlined in Scheme 1, stoichiometric one-electron reduction of [Tp′(CO)(L)M(η^2-BnSC$_2$SBn)](PF$_6$) (Tp′ = hydrotris(3,5-dimethylpyrazolyl)borate, Bn = benzyl, M = W, L = CO (**1a**), M = Mo, L = 2,6-Me$_2$C$_6$H$_3$NC (**1b**), M = Mo, L = *t*-BuNC (**1c**)) led to the neutral complexes [Tp′(CO)(L)M(η^2-BnSC$_2$S)] (M = W, L = CO (**2a**), M = Mo, L = 2,6-Me$_2$C$_6$H$_3$NC (**2b**), M = Mo, L = *t*-BuNC (**2c**)), which were isolated in 50−70% yield by chromatography and subsequent crystallization.[8,11] Reaction of analytically pure **2a**/**2b**/**2c** with 1 equiv of C_8K in THF at −78 °C resulted in intensely colored solutions. Upon warming to ambient temperature, the solutions turned red-brown, and the potassium salts K[Tp′(CO)(L)W(η^2-C$_2$S$_2$)] (M = W, L = CO (K-**3a**), M = Mo, L = 2,6-Me$_2$C$_6$H$_3$NC (K-**3b**), M = Mo, L = *t*-BuNC (K-**3c**)) were precipitated.

The identity of K-**3a**, K-**3b**, and K-**3c** was proven by IR, ESI-MS, and particularly ^{13}C NMR spectroscopy (Table 2). The CO stretching frequencies of K-**3a** are shifted to lower energy with respect to **2a** by 34 and 25 cm^{-1}, respectively. In contrast, the increased π backbonding in the isocyanide complexes K-**3b** and K-**3c** with respect to the neutral complexes **2b** and **2c** mostly affects the C≡N vibration. Generally, the mean frequency change of the CO/CN vibrations is halved in the second reduction step (K-**3** with respect to **2**) compared with the first benzyl removal (**2** with respect to **1**-PF$_6$). Obviously, the additional charge in K-**3a** is predominantly localized at the sulfur atoms, while the loss of positive charge going from **1a**-PF$_6$ to **2a** is much more effective at the metal center itself. The retention of the overall complex topology is reflected in the ^{13}C NMR spectra. Alkyne resonances could not be detected in the room-temperature spectrum of K-**3a** in THF-d_8 by virtue of the alkyne rotation at the metal center. However, two alkyne resonances are observed for K-**3a** at −60 °C, while two alkyne resonances are already found in the room-temperature spectra of K-**3b** and K-**3c** in CD_3CN. The large shift difference (291 vs 252 ppm in K-**3a**, 294 vs 270 ppm in K-**3c**) and the very low field shift of the alkyne resonances

Scheme 1. Synthesis of Metalla-Acetylendithiolate Ligands[a]

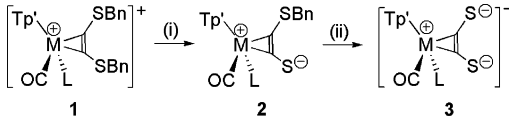

1 2 3

M = W, L = CO **1a**, **2a**, **3a**
M = Mo, L = 2,6-Me$_2$C$_6$H$_3$NC **1b**, **2b**, **3b**
M = Mo, L = *tert*-BuNC **1c**, **2c**, **3c**

[a] Reagents: (i) [(η^5-C$_5$H$_5$)$_2$Co]/THF; (ii) C_8K/THF.

(16) (a) Ahlrichs, R.; Bär, M.; Häser, M.; Horn, H.; Kölmel, C. *Chem. Phys. Lett.* **1989**, *162*, 165. (b) Häser, M.; Ahlrichs, R. *J. Comput. Chem.* **1989**, *10*, 104. (c) von Arnim, M.; Ahlrichs, R. *J. Comput. Chem.* **1998**, *19*, 1746.
(17) (a) Becke, A. D. *Phys. Rev. A*: *At., Mol., Opt. Phys*. **1988**, *38*, 3098. (b) Perdew, J. P. *Phys. Rev. B: Condens. Matter Mater. Phys.* **1986**, *33*, 8822. Erratum: Perdew, J. P. *Phys. Rev. B: Condens. Matter Mater. Phys.* **1986**, *34*, 7406.
(18) (a) Treutler, O.; Ahlrichs, R. *J. Chem. Phys.* **1995**, *102*, 346. (b) Eichkorn, K.; Treutler, O.; Öhm, O.; Häser, M.; Ahlrichs, R. *Chem. Phys. Lett.* **1995**, *240*, 283. (c) Eichkorn, K.; Weigend, F.; Treutler, O.; Ahlrichs, R. *Theor. Chem. Acc.* **1997**, *97*, 119.
(19) (a) Eichkorn, K.; Treutler, O.; Öhm, O.; Häser, M.; Ahlrichs, R. *Chem. Phys. Lett.* **1995**, *242*, 652. (b) Haase, F.; Ahlrichs, R. *J. Comput. Chem.* **1993**, *14*, 907. (c) Weigend, F.; Häser, M. *Theor. Chem. Acc.* **1997**, *97*, 331. (d) Weigend, F.; Häser, M.; Patzelt, H.; Ahlrichs, R. *Chem. Phys. Lett.* **1998**, *294*, 143.
(20) Schäfer, A.; Horn, H.; Ahlrichs, R. *J. Chem. Phys.* **1992**, *97*, 2571.
(21) Deglmann, P.; Furche, F.; Ahlrichs, R. *Chem. Phys. Lett.* **2002**, *362*, 511.
(22) (a) Bauernschmitt, R.; Häser, M.; Treutler, O.; Ahlrichs, R. *Chem. Phys. Lett.* **1997**, *264*, 573. (b) Bauernschmitt, R.; Ahlrichs, R. *Chem. Phys. Lett.* **1996**, *256*, 454. (c) Bauernschmitt, R.; Ahlrichs, R. *J. Chem. Phys.* **1996**, *104*, 9047. (d) Weiss, H.; Ahlrichs, R.; Häser, M. *J. Chem. Phys.* **1993**, *99*, 1262. (e) Furche, F.; Ahlrichs, R.; Wachsmann, C.; Weber, E.; Sobanski, A.; Vögtle, F.; Grimme, S. *J. Am. Chem. Soc.* **2000**, *122*, 1717. (f) Furche, F. *Dichtefunktionalmethoden für elektronisch angeregte Zustände*, Dissertation, Universität Karlsruhe, Germany, 2002.

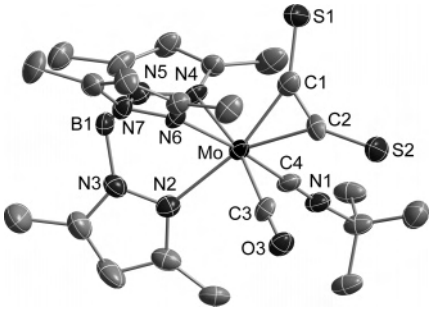

Figure 1. Molecular structure of the anion **3c**$^-$; hydrogen atoms are omitted; 50% ellipsoid probability.

Scheme 2. Synthesis of Metalla-Acetylendithiolato Complexes

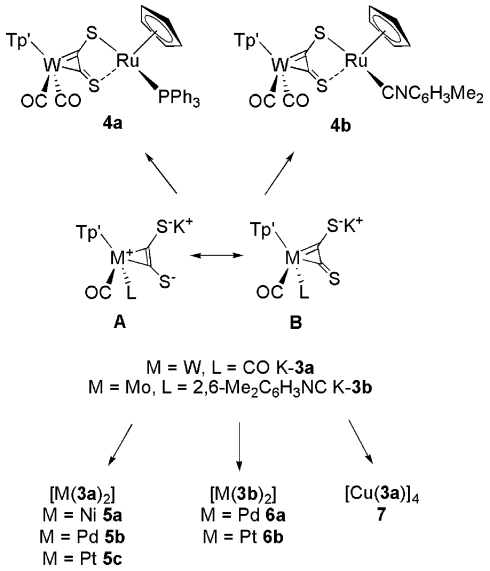

with respect to reference values of W/Mo(II) four-electron donor alkyne complexes (cf. 180−240 ppm)[23] point to the contribution of resonance structure **B** (Scheme 2) displaying a thioketo function.

The identity of K-**3c** was confirmed by single-crystal X-ray diffraction. A representation of the solid-state structure is presented in Figure 1, and selected metrical parameters are reported in Table 3. The potassium salt K-**3c** forms a tetramer, in which the transition-metal complex anions are connected by electrostatic sulfur−potassium contacts in the range of 3.116−3.176 Å. The molecular structure of the anion **3c**$^-$ shows a roughly octahedral complex, considering the alkyne occupying a single coordination site. The alkyne SC_2S-plane (torsion angle S1−C1−C2−S2 = 6.3°) lies between the CO and the isocyanide, but tilted to the CO vector (torsion angle C3−Mo−C1−C2 = 22.0°). The C1−S1 and C2−S2 bond distances of 1.668(8) and 1.670(7) Å are equal within the margin of error. The difference in the Mo−C1 and Mo−C2 bond distances (2.056(8) vs 2.108(7) Å) reflects contributions of resonance structure **B** (see Scheme 2), but it is smaller compared with the differences found in the neutral complexes **2a**/**2b**/**2c**.[8,11] The bend-back angles of 143.8° (C1−C2−S2) and 138.3° (C2−C1−S1), respectively, give rise to an intramolecular S1−S2 distance of 3.899 Å, which is far too large for a chelate coordination.

(23) Templeton, J. L. *Adv. Organomet. Chem.* **1989**, *29*, 1−100.

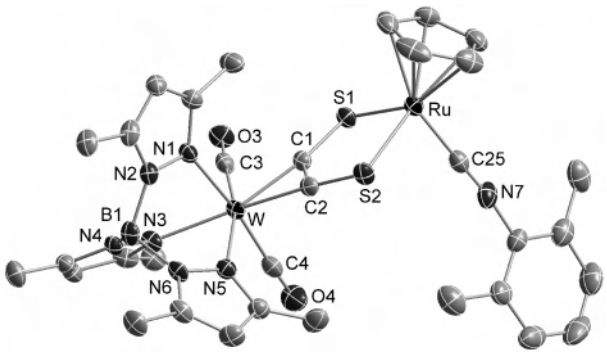

Figure 2. Molecular structure of **4b**; hydrogen atoms are omitted; 50% ellipsoid probability.

Table 3. Selected Bond Lengths (Å) and Angles (deg) in K-**3c** and **4b**

	K-**3c** (M = Mo)	**4b** (M = W)
Ru−S1		2.388(1)
Ru−S2		2.378(1)
C1−S1	1.668(8)	1.675(5)
C2−S2	1.670(7)	1.669(5)
C1−C2	1.303(10)	1.381(7)
M−C1	2.056(8)	2.051(5)
M−C2	2.108(7)	2.037(5)
C1−C2−S2	143.8(6)	121.5(4)
C2−C1−S1	138.3(7)	126.9(4)
S1−Ru−S2		86.3(5)

Heterobimetallic Tungsten−Ruthenium Complexes. The reaction of K-**3a** with $[(\eta^5\text{-}C_5H_5)Ru(L)(CH_3CN)_2](PF_6)$ (L = PPh_3, 2,6-$Me_2C_6H_3NC$) at room temperature (Scheme 2) afforded intensely blue **4a** (L = PPh_3) and **4b** (L = 2,6-$Me_2C_6H_3NC$), which were isolated in analytically pure form by column chromatography and subsequent crystallization. The structure determination of **4b** (Figure 2 and Table 3) disclosed a bridging acetylenedithiolate ligand, which coordinates the tungsten complex entity in a η^2-C,C′ mode and the ruthenium complex fragment in a chelatelike k^2 fashion by the sulfur atoms. A similar structure has been reported earlier for the compound **4a**.[9a] The similarity of both structures clearly reveals that steric protection by the bulkier PPh_3 in **4a** is not crucial for a stabilization of the μ-η^2-C,C′-k^2-S,S′ binding mode of acetylenedithiolate. The planarity of the five-membered chelate ring is reflected in the angle sum of 539.5° with an acute S1−Ru−S2 angle of 86.3°. The C1−C2 bond of 1.381(7) Å is significantly longer compared with the corresponding C1−C2 bond of 1.303(10) Å in K-**3c**. The bend-back angles C1−C2−S2 and C2−C1−S1 of 121.5° and 126.8°, respectively, are close to the ideal value of 120° for sp^2 carbon atoms leading to an intramolecular S1−S2 distance of 3.26 Å. The comparison of the bend-back angles in **4a**/**4b** and K-**3c** emphasizes that the decreased angles in **4a**/**4b** are a direct consequence of the chelate ring formation. The W−C1/W−C2 and the C1−S1/C2−S2 distances are equal within experimental error, which is reflected in resonance structure **A**. Additionally, the difference of the two bend-back angles and the difference of the two ruthenium−sulfur bond lengths is smaller in **4b** compared with the corresponding values in **4a**,[9a] indicating either a larger contribution of resonance structure **A** or a higher degree of delocalization **B**′/**B**″ in **4b** (Chart 1).

Chart 1

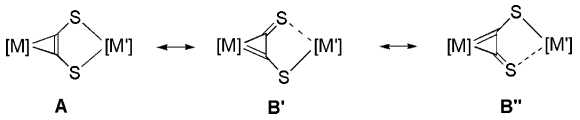

In this context, the small increase of the CO stretching frequencies going from K-**3a** to **4a**/**4b** implies that charge transfer from tungsten to sulfur (accompanied by a shift of resonance structure **B** to **A**) as a result of the coordination of the sulfur atoms at the ruthenium complex fragment is generally small. A subtle change of the contributions of the resonance structures from **B** to **A**, however, is evident from the more distinct increase of the CO stretches going from K-**3a** to **4b** as compared with **4a**. The π-acceptor ability of the isocyanide ligand renders the ruthenium center more Lewis-acidic, which give rise to a higher charge transfer from tungsten to the bridging acetylenedithiolate ligand.

The fluxional behavior of the alkyne ligand at the metal, which is evident in K-**3a**/K-**3b**/K-**3c**, was quantified with **4a**/**4b**. Variable-temperature ^{1}H and ^{13}C NMR measurements revealed a roughly 90° rotation of the Tp′W(CO)$_2$ unit at the alkyne rendering the CO ligands and the alkyne carbon atoms indistinguishable. The difference of the activation barriers determined to $\Delta G°_{298} = 48.8$ kJ/mol for **4a** and to $\Delta G°_{298} = 47.2$ kJ/mol for **4b** by line shape analysis[9a] reflects the influence of the ligand type at ruthenium on the electronic situation at tungsten. Both these NMR measurements and the IR spectroscopic investigations underline the polarizability of the metalla-acetylenedithiolate ligand. The two ^{13}C NMR resonances of the alkyne carbon atoms in **4b** were detected at −60 °C at 278 and 261 ppm. The reduced shift difference ($\Delta\delta = 17$ ppm) compared with the corresponding resonances in **3a**$^-$ ($\Delta\delta = 39$ ppm) reveals the increased electronic similarity of both alkyne carbon atoms in the heterobimetallic complex **4b**. Generally, the observed changes of the ^{13}C NMR shifts of the alkyne carbon atoms resulting from coordination at the sulfur atoms are small. Consequently, coordination of ruthenium at the sulfur atoms and the corresponding change of the bend-back angle do not dramatically alter the bonding in the alkyne complex moiety.

Interestingly, product **4a** is also obtained from K-**3a** and [(η^5-C$_5$H$_5$)Ru(PPh$_3$)$_2$Cl]. Reaction at ambient temperature led to an intense green solution displaying a ^{31}P NMR resonance at $\delta_P = 41.3$ ppm. This signal is assigned to the intermediate [(η^5-C$_5$H$_5$)Ru(PPh$_3$)$_2$(**3a**)], which is transformed into blue **4a** ($\delta_P = 55.9$ ppm) by intramolecular substitution under reflux conditions. The substitution of a phosphine ligand at ruthenium points to a strong tendency of chelate ring formation with **3a**$^-$.

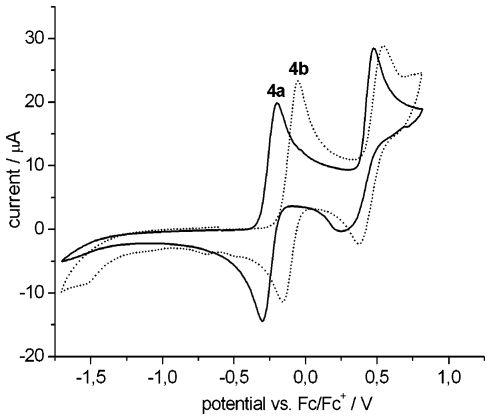

Figure 3. Cyclic voltammograms of **4a** (solid line) and **4b** (dotted line) in CH_2Cl_2 (scan rate 100 mV·s^{-1}).

Stability in more than one oxidation state is a typical feature of dithiolene complexes.[24] In addition, the extensive work of Connelly et al. has proven the versatile redox activity of the [Tp′M(L)$_2$(alkyne)] (M = Mo, W) complex moiety.[25] Indeed, according to cyclic voltammetry studies, **4a**/**b** undergo a reversible electron transfer at moderate potential and a second irreversible oxidation in the case of **4a** and a quasi-reversible redox process in the case of **4b** at a potential above Fc/Fc$^+$ (Figure 3). The first electron transfer, which is observed at $E_{1/2} = -250$ mV for **4a** and at $E_{1/2} = -110$ mV for **4b** (referenced against Fc/Fc$^+$), depends significantly on the substitution at ruthenium. Therefore, the oxidation is tentatively assigned as ruthenium-based since the π-acidic isocyanide reasonably stabilizes Ru(II). However, the stoichiometric oxidation of **4a** with [(η^5-C$_5$H$_5$)$_2$Fe](PF$_6$) yielding the corresponding complex **4a**-PF$_6$ caused a remarkable increase of the stretching frequencies of the tungsten-bound CO ligands ($\Delta\nu = 51$ and 57 cm^{-1}). Indeed, the oxidation potential of **4a**/**4b** falls in the range, which was determined for related neutral complexes [TpW(CO)(X)(PhC$_2$Ph)] (X = halide) by Connelly et al.[25b] The corresponding oxidation of **4b** to **4b**-PF$_6$ led to both a comparable frequency increase for the tungsten-bound CO ligands ($\Delta\nu = 50$ and 52 cm^{-1}) and for the ruthenium-coordinated isocyanide ($\Delta\nu = 88$ cm^{-1}). Accordingly, the one-electron oxidation affects both metal centers to a comparable degree, which indicates a highly delocalized highest occupied molecular orbital (HOMO) for **4a**/**4b**.

This perception is contradicted by EPR spectroscopic measurements on paramagnetic **4a**$^+$/**4b**$^+$ (Figure 4). In a frozen solution of **4a**$^+$, a hyperfine coupling to phosphorus displaying moderate anisotropy is apparent from the low-temperature spectrum at X-band frequency. By comparison, the spectrum of **4b**$^+$ reveals a rhombic g tensor with broad

(24) Wang, K. *Prog. Inorg. Chem.* **2004**, *52*, 267−314.
(25) (a) Adams, C. J.; Connelly, N. G.; Onganusorn, S. *Dalton Trans.* **2007**, 1904−1910. (b) Adams, C. J.; Bartlett, I. M.; Carlton, S.; Connelly, N. G.; Harding, D. J.; Hayward, O. D.; Orpen, A. G.; Patron, E.; Ray, C. D.; Rieger, P. H. *Dalton Trans.* **2007**, 62−72. (c) Adams, C. J.; Bartlett, I. M.; Boonyuen, S.; Connelly, N. G.; Harding, D. J.; Hayward, O. D.; McInnes, E. J. L.; Orpen, A. G.; Quayle, M. J.; Rieger, P. H. *Dalton Trans.* **2006**, 3466−3477. (d) Adams, C. J.; Anderson, K. M.; Connelly, N. G.; Harding, D. J.; Orpen, A. G.; Patron, E.; Rieger, P. H. *Chem. Commun.* **2002**, 130−131.
(26) (a) Paul, F.; Ellis, B. G.; Bruce, M. I.; Toupet, L.; Roisnel, T.; Costuas, K.; Halet, J.-F.; Lapinte, C. *Organometallics* **2006**, *25*, 649−665. (b) Heck, J.; Lange, G.; Malessa, M.; Boese, R.; Blaser, D. *Chem.—Eur. J.* **1999**, *5*, 659−668. (c) DeSimone, R. E. *J. Am. Chem. Soc.* **1973**, *95*, 6238−6244. (d) Connelly, N. G.; Manners, I.; Protheroe, J. R. C.; Whitely, M. W. *J. Chem. Soc., Dalton Trans.* **1984**, 2713−2717. (e) Castellani, M. P.; Connelly, N. G.; Pike, R. D.; Rieger, A. L.; Rieger, P. H. *Organometallics* **1997**, *16*, 4369−4376. (f) Pike, R. D.; Rieger, A. L.; Rieger, P. H. *J. Chem. Soc., Faraday Trans. 1* **1989**, *85*, 3913−3925.

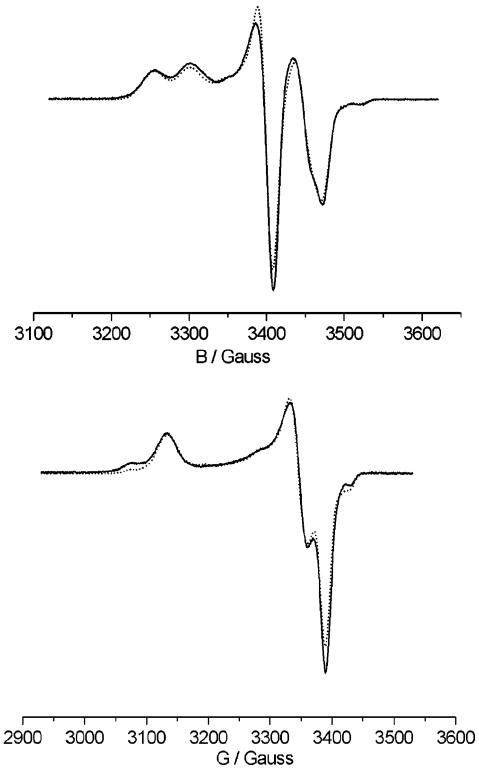

Figure 4. EPR spectra of **4a**-PF_6 (top) and **4b**-PF_6 (bottom) in a frozen THF/CH_2Cl_2 solution at X-band frequency (measured, solid line; calculated, dotted line).

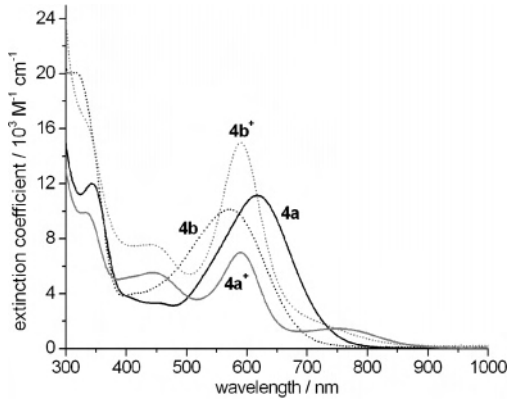

Figure 5. Electronic spectra of **4a** (black line), **4a**$^+$ (gray line), **4b** (black line, dotted) and **4b**$^+$ (gray line, dotted) in CH_2Cl_2.

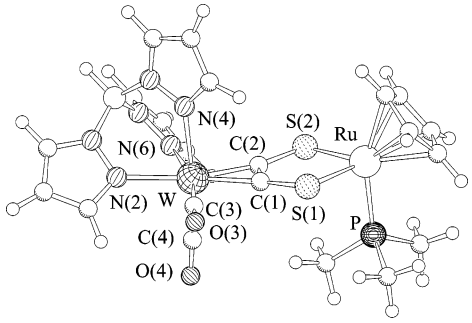

Figure 6. Geometry-optimized structure of **4a′** and numbering scheme used.

satellites arising from the $^{99}Ru/^{101}Ru$ ($I = {}^5/_2$) hyperfine coupling. The g values and hyperfine coupling constants obtained by simulation of the spectra are related to literature data in Table 4.[25a,26] The small difference between the g_2 and g_3 values leads to the asymmetric doublet structure, which is apparent in the high-field part of the spectrum of **4a**$^+$. The comparatively high a_p values, which reflect some dipolar coupling, point to a singly occupied molecular orbital (SOMO), which is predominantly localized at ruthenium. In addition, the g-value anisotropy in **4a**$^+$/**4b**$^+$ is consistent with a sulfur-coordinated Ru(III) center. Finally, the increase of the g anisotropy going from **4a** to **4b** precludes a tungsten-based single electron because the tungsten environment is retained.

The putative inconsistency of a highly delocalized HOMO in the neutral complexes **4a**/**4b** and a ruthenium-based SOMO in the cations **4a**$^+$ and **4b**$^+$ can be resolved by comparison of the electronic spectra (Figure 5). While a hypsochromic shift of the strong charge-transfer band at 618 nm owing to the oxidation is evident for **4a**, the opposite is observed for **4b**. This converse behavior gives rise to very similar absorptions for **4a**$^+$ and **4b**$^+$ ($\Delta\lambda = 2$ nm), while the absorption maxima of **4a** and **4b** differ by 47 nm. Thus, the influence of the ruthenium-bound ligand L on the relevant visible absorption is pronounced in the neutral complexes and negligible in the cations. Therefore, a significant change of the frontier orbital composition as a result of the oxidation is likely.

DFT Calculations. In order to substantiate the conclusions drawn from spectroscopic data, DFT calculations have been performed on the complexes [{Tp′$(CO)_2$W}(η^2-C_2S_2){Ru(L)(η^5-C_5H_5)}] (L = PPh_3, 2,6-$Me_2C_6H_3NC$) (**4a/b**), on their slightly reduced model compounds [{Tp$(CO)_2$W}(η^2-C_2S_2){Ru(PMe_3)(η^5-C_5H_5)}] (**4a′**) and [{Tp$(CO)_2$W}(η^2-C_2S_2){Ru(NCPh)(η^5-C_5H_5)}] (**4b′**) (Tp = hydrotris(pyrazolyl)borate), as well as on the monocations of these complexes. For compounds **4a** and **4b**, the optimized geometries are in considerable agreement with the experimentally determined structures. To clarify the numbering scheme used in the following, the geometry-optimized structure of **4a′** is given in Figure 6. The important metrical parameters of the central dimetalla-acetylenedithiolate entity of the geometry-optimized complexes **4a**/**4b** and their cations are given in Table 5.

Each of the calculated structures comprises the μ-η^2-C,C′-k^2-S,S′ binding mode of the acetylenedithiolate ligand in the complexes, featuring a planar, five-membered chelate ring with the ruthenium atom. The angles S1−Ru−S2 vary in a narrow range between 85.40° and 86.22° for the neutral complexes and 87.83° and 88.84° for the cations. The angle calculated for **4b** (86.20°) is, within experimental error, identical to the corresponding angle observed for the molecular structure of this compound (86.3°). Similarly, the different bend-back angles of C1−C2−S2 and C2−C1−S1 are well-resolved in the calculated structures. The calculated C1−C2 bond distances are almost invariant to the charge of the complexes, which we calculate as 1.3806 to 1.3848 Å, compared to 1.381(8) Å observed in the molecular structure of **4b**. Upon oxidation, however, a reduction of the ruthenium−sulfur distances is predicted. The concomitant changes for the tungsten−carbon and carbon−sulfur distances are

Table 4. EPR Data of [**4a**$^+$](PF$_6$) and [**4b**$^+$](PF$_6$) in Frozen CH_2Cl_2/THF Solution and Related Complexes

	g_i	$a_i(^{31}P)$/G	$a_i(^{99}Ru/^{101}Ru)$/G
[**4a**$^+$](PF$_6$)	2.103/2.012/2.005 $\langle g\rangle = 2.038$	70/43/46	18/-/-
[**4b**$^+$](PF$_6$)	2.150/2.014/1.988 $\langle g\rangle = 2.052$		15/19/22
[Ru(η^5-C_5Me_5)(dppe)(C_2Ph)][26a] [a]	2.333/2.067/1.971 $\langle g\rangle = 2.123$	not resolved	not resolved
[Ru(η^5-C_5H_5)]$_2$(μ-cot)[26b] [b]	2.322/2.164/1.982 $\langle g\rangle = 2.052$		not resolved
[Ru(dtc)$_3$][26c] [c]	2.156/2.109/1.979 $\langle g\rangle = 2.052$		38/21
[Ru(CO)$_2$(PPh_3)$_2$($O_2C_6Cl_4$)]$^+$ [26d]	$\langle g\rangle = 2.002$	$\langle a\rangle = 25.1$	$\langle a\rangle = 3.7$
[Tp′Mo(CO)(PhC_2Ph)(μ-CN)-Ru(CO)$_2$(PPh_3)($O_2C_6Cl_4$)]$^+$ [25a]	$\langle g\rangle = 2.0032$	$\langle a\rangle = 21.7$	$\langle a\rangle = 2.6$

[a] dppe = bis(diphenylphosphino)ethane. [b] cot = cyclooctatetraene. [c] dtc = diethyldithiocarbamate.

Table 5. Metric Parameters of the Central Dimetalla-Acetylenedithiolate Unit in the Calculated Structures of Complexes **4a**/**4b** and Their Cations

	4a	**4a**$^+$	**4b**	**4b**$^+$
W−C1	2.1130	2.0930	2.1060	2.0923
W−C2	2.0871	2.0771	2.0768	2.0764
Ru−S1	2.4131	2.3773	2.4136	2.3844
Ru−S2	2.4061	2.3618	2.4175	2.3740
C1−C2	1.3827	1.3809	1.3834	1.3795
C1−S1	1.6892	1.6982	1.6862	1.6940
C2−S2	1.6949	1.7016	1.6944	1.7010
S1−S2	3.2683	3.2879	3.3008	3.3154
C1−C2−S2	121.496	121.786	122.157	122.350
C2−C1−S1	126.193	126.423	126.924	127.168
S1−Ru−S2	85.403	87.862	86.197	88.333

smaller, the former being shorter and the latter being longer in the cationic complexes.

Important frontier orbitals of **4a** are given in Figure 7. The lowest unoccupied molecular orbital (LUMO) of the complex reveals the main contributions of the acetylenedithiolate ligand and of one of the CO ligands and the minor contributions at the tungsten and ruthenium atoms. The HOMO is characterized by the balanced contributions of both metal atoms, whereas the orbitals HOMO-1 and HOMO-2 are centered at the ruthenium atom while HOMO-3 is centered at the tungsten atom of the dinuclear complex.

Due to the lowered electron density of the cations **4a**$^+$ and **4b**$^+$, the calculated carbonyl stretches increase by 50−60 cm^{-1}, depending on the nature of the co-ligands and the model employed. For complex **4a**, we calculate carbonyl stretching frequencies at 1922 and 1992 cm^{-1} (experimentally observed at 1910 and 1984 cm^{-1}), whereas the cationic complex reveals these resonances at 1979 and 2031 cm^{-1} (experimentally observed at 1967 and 2035 cm^{-1}). For the isonitrile-stabilized complex **4b**, the calculated carbonyl stretching frequencies are at 1939 and 1999 cm^{-1} (experimentally observed at 1918 and 1988 cm^{-1}) and the CN stretch of the isocyanide ligand at 2089 cm^{-1} (experimentally observed at 2056 cm^{-1}). For the cationic complex **4b**$^+$, these stretching frequencies are calculated to be at 1986, 2035, and 2133 cm^{-1} (experimentally observed at 1970, 2038, and 2143 cm^{-1}).

The one-electron oxidation process mainly affects the HOMO of the complexes, which contains significant character at the ruthenium, tungsten and sulfur atoms, as shown for **4a** in Figure 7. Close in energy, however, are the two predominantly at the ruthenium atom localized orbitals HOMO-1 and HOMO-2. For the cations of these compounds, we recognize a slight mixing of these orbitals as compared with the neutral species, especially of HOMO-2 into the HOMO of the complex. The spin densities ($\alpha-\beta$) calculated for the cations of **4a**$^+$ and **4b**$^+$ show a major contribution at the ruthenium atom (Figure 8) and thus nicely support the conclusions drawn from EPR spectroscopy.

To gain more insight into the nature of the electronic transitions, TDDFT singlet excitation energies of all complexes have been calculated. For **4a**, we obtain three transitions with high oscillator strengths at 729 nm (oscillator strength 0.039), 627 nm (0.142), and 591 nm (0.0052). The transition of highest strength at 627 nm is close to the experimentally observed maximum in the UV−vis spectrum of this compound at 618 nm. The calculated singlet excitations at 729 and 627 nm predominantly result from excitations out of HOMO (44.5 and 47.4%) and HOMO-2 (54.1 and 44.3%) into the LUMO of **4a**. Since the LUMO predominantly contains major contributions of the acetylenedithiolate ligand and the tungsten carbonyl moiety and minor contributions of ruthenium d orbitals, whereas HOMO and HOMO-2 significantly contain ruthenium d character, this transition may be regarded as a charge transfer from ruthenium to the tungsten acetylenedithiolate unit of the molecule. The transition at 591 nm stems exclusively from an excitation out of HOMO-3, which is tungsten-centered into the LUMO of the complex. Therefore, the experimentally band observed at 618 nm is, according to our calculations, a metal-to-ligand charge transfer (MLCT), in which both metal atoms of the dinuclear complex are involved. For the isocyanide complex **4b**, all relevant calculated transitions have mixed character. They can also be characterized as MLCT excitations out of ruthenium- or tungsten-centered orbitals into the LUMO of the complex. For these compounds, orbital shape and ordering of the frontier orbitals is similar to those depicted for **4a** in Figure 7, albeit the orbitals HOMO to HOMO-4 are lower in energy due to the π-accepting properties of the isonitrile and the good σ-donor properties of the phosphine ligand. For **4b**, we calculate transitions at 688 nm (0.039), 598 nm (0.025), and 587 nm (0.125), which also compare well with a maximum at 587 nm observed experimentally in the UV−vis spectrum of **4b**.

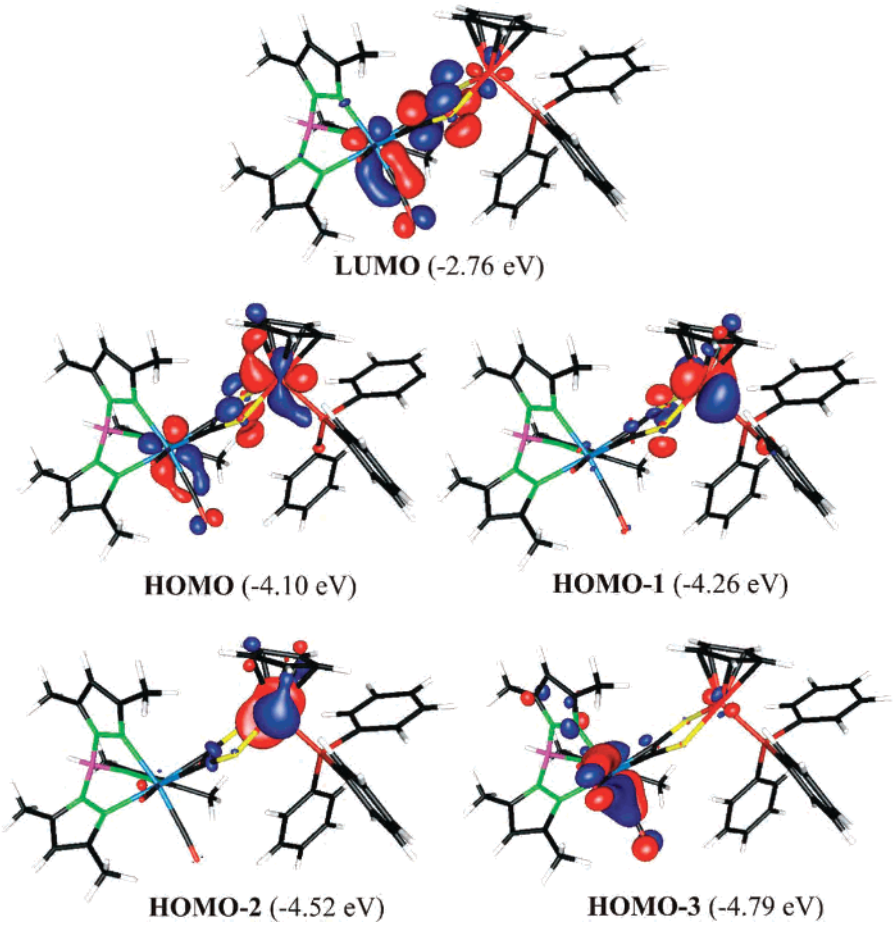

Figure 7. Important frontier orbitals of **4a**.

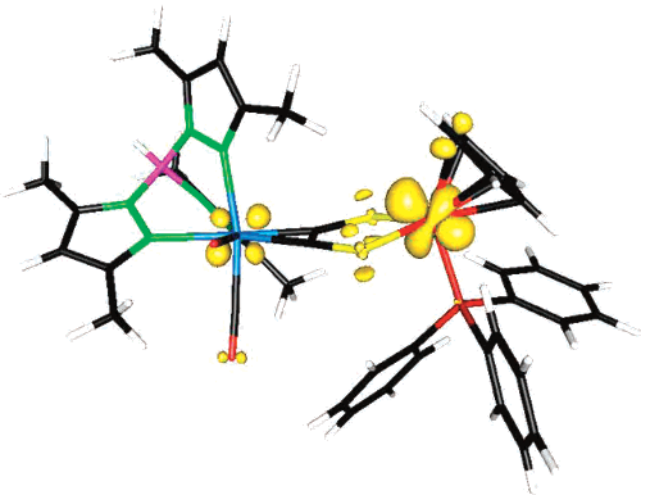

Figure 8. Spin density calculated for $\mathbf{4a}^{+}$.

Homoleptic Complexes of $\mathbf{3a}^{-}$ and $\mathbf{3b}^{-}$ with Group 10 Metal Ions. Intensely colored complexes of type $[M(\mathbf{3a})_2]$ (M = Ni (**5a**), Pd (**5b**), Pt (**5c**)) and $[M(\mathbf{3b})_2]$ (M = Pd (**6a**), Pt (**6b**)) were synthesized from K-**3a**/K-**3b** in THF/CH_2Cl_2 or THF/CH_3CN solvent mixtures using $[Ni(NCMe)_6](BF_4)_2$, $[Pd(NCMe)_4](BF_4)_2$, and $[PtCl_2(NCPh)_2]$, respectively, as starting materials (Scheme 2). In all cases, the complex formation is indicated by a color change to either blue (Ni, Pt) or red (Pd) and by a distinct increase of the CO and CN streching frequencies of the carbonyl and isocyanide ligands ($\Delta\nu$ = 33 to 50 cm^{-1}). Despite several attempts, the nickel congener $[Ni(\mathbf{3b})_2]$ could not be isolated. Crystalline, analytically pure samples of all the complexes could only be obtained after column chromatography and direct crystallization from the eluated toluene solutions. The molecular structures of **5a**, **5b**, and **5c** have already been discussed in a preceding communication.[9b] The crystals of **6a** and **6b** are isomorphous, revealing the similarity of the overall molecular structures. A representation of the solid-state structure of **6b** is presented in Figure 9, and selected metrical parameters of **6a** and **6b** are reported in Table 6. The central metal ions, which lie on an inversion center, are coordinated by two metalla ligands $\mathbf{3b}^{-}$ in a square-planar fashion as observed in **5a**/**5b**/**5c**. Both C_2S_2M chelate rings are planar and coplanar to each other, leading to a planar bridge between both molybdenum centers. The isocyanide ligands are coordinated perpendicular to this plane, while the remaining carbonyl ligands adopt the in-plane position. The bend-back angle of the sulfur substituents in the molybdenum alkyne complex moieties of **6a** and **6b** is somewhat smaller compared with that of **5a**/**5b**/**5c**,[9b] which leads to a longer intramolecular S1−S2 distance (3.2702(21) Å in **5c** and 3.2934(11) Å in **6b**). This effect probably accounts for the instability of the complex $[Ni(\mathbf{3b})_2]$ because the short Ni−S distances require the strongest bend-back angles in the alkyne complex moiety. The comparison of the bond lengths within the chelate rings, M−S1, S1−C1, and C1−Mo with M−S2,

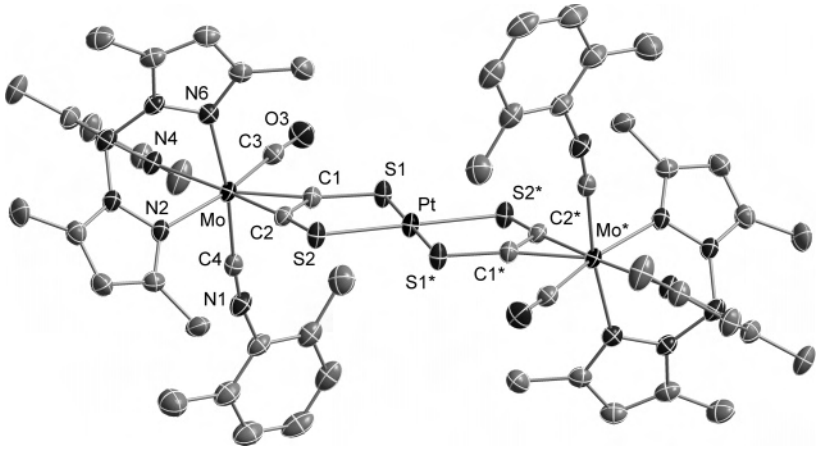

Figure 9. Molecular structure of **6b**; hydrogen atoms are omitted; 50% ellipsoid probability.

Table 6. Selected Bond Lengths (Å) and Angles (deg) in **6a** and **6b**

	Pd	Pt		Pd	Pt
M−S1	2.3284(9)	2.3167(9)	Mo−C2	2.010(3)	2.009(3)
M−S2	2.3368(8)	2.3249(9)	C1−C2−S2	123.8(2)	122.3(3)
C1−S1	1.685(3)	1.689(4)	C2−C1−S1	128.5(3)	127.8(3)
C2−S2	1.693(3)	1.689(3)	S1−M−S2	91.25(3)	90.39(3)
C1−C2	1.341(5)	1.351(5)	S1−M−S2*	88.75(4)	89.61(3)
Mo−C1	2.031(3)	2.023(3)			

S2−C2, and C2−Mo, respectively, reveals significant differences solely for the M−S distances, reflecting the difference in the bend-back angles. Therefore, a high degree of delocalization is evident from the structural data, if resonance structure **B** (Scheme 2) is considered as the dominant contribution. This observation essentially substantiates similar results for **5a**/**5b**/**5c** because of the higher accuracy of the structure solution for **6a** and **6b**. In fact, as similarly concluded for **5a**/**5b**/**5c**, the sulfur coordination in **6a** and **6b** adopts a typical dithiolene structure. However, the M−S bond lengths (Table 6) fall at the very high end for dithiolene complexes and they are distinctly longer than those in neutral dithiolene complexes (compare $[(Ph_2C_2S_2)_2Pt]$ of 2.246 and 2.244 Å and $[\{(t\text{-}BuC_6H_4)_2C_2S_2\}_2Pd]$ of 2.251(1) Å).[27] The observed M−S bond lengths are rather typical for homoleptic bis(dithiocarbamato) complexes (compare $[(Et_2NCS_2)_2Pd]$ of 2.330 and 2.325 Å).[28] The substitution of one carbonyl ligand in **5b**/**5c** by an isocyanide and the change from tungsten to molybdenum does not significantly influence the Pd−S and the Pt−S bond lengths.

The determination of the particularly indicative ^{13}C NMR shifts of the alkyne carbon atoms turned out to be impossible in **5a**/**5b**/**5c**. We attribute these difficulties to the coalescence of the alkyne signals at room temperature due to the alkyne rotation at tungsten. However, at low temperatures we encountered serious solubility problems. We have recently shown that weaker π-acidic ligands like isocyanides in the alkyne complex distinctively lower the rotational barrier of the alkyne.[11] Consistently, a single alkyne carbon resonance was observed in the room-temperature ^{13}C NMR spectrum of **6a** and **6b**. The resonance at 268 ppm for **6b** is close to the mean value of the two low-temperature resonances observed in **4a**. Therefore, a comparable electronic situation in the alkyne complex moieties of $\mathbf{3a}^-$ and $\mathbf{3b}^-$ in their S,S′-chelate complexes can be concluded.

Recent comprehensive re-evaluations of the electronic structure of nickelbis(ethylenedithiolate) and metalbis(benzenedithiolate) (M = Ni, Pd, Pt) complexes substantiated that the diamagnetic neutral compounds consist of divalent metal centers (nd^8, $S_M = 0$) and two S,S′-coordinated dithio-(1−) π radical anions.[29] The two spins are antiferromagnetically coupled via a superexchange mechanism mediated through the diamagnetic metal(II) ion. Accordingly, the oxidation state of II is assigned to the central metals in **5a**/**5b**/**5c** and **6a**/**6b**. However, due to the electronic conjugation to tungsten, a radical formulation is not appropriate as indicated by the resonance structure **B** for the metalla-acetylenedithiolate ligands (Scheme 2). This difference to the electronic structure of typical dithiolene complexes is reflected in the UV−vis spectra. Complexes with 1,2-dithiosemiquinonate(1−) π radical anions consistently show an intense band between 800 and 900 nm, which reveals only little variation upon exchange of the central metal ion.[29b] These transitions are consequently assigned to a ligand-to-ligand charge transfer. Likewise, complexes **5a**/**5b**/**5c** and **6a**/**6b** exhibit an intense band in the visible range of the spectra (Figure 10). However, this absorption is remarkably shifted to higher energy upon exchange of the central metal ion in the order Ni in **5a** (649 nm), Pt in **5c** (599 nm), and Pd in **5b** (501 nm). In contrast, the transitions vary only little, if the metalla-acetylenedithiolate ligand $\mathbf{3a}^-$ is replaced by $\mathbf{3b}^-$. This observation indicates a significant contribution of the central metal d orbitals in the transition.

However, standard ligand-to-metal charge-transfer bands in related square-planar complexes with dithiocarbamato ($R_2NCS_2^-$), xanthato ($ROCS_2^-$), or dithiophosphinato ($R_2PS_2^-$) ligands are observed at much higher energy following the

(27) (a) Dessy, G.; Fares, V.; Bellitto, C.; Flamini, A. *Cryst. Struct. Commun.* **1982**, 1743−1745. (b) Kokatam, S.; Ray, K.; Pap, J.; Bill, E.; Geiger, W. E.; LeSuer, R. J.; Rieger, P. H.; Weyermüller, T.; Neese, F.; Wieghardt, K. *Inorg. Chem.* **2007**, *46*, 1100−1111.

(28) (a) Beurskens, P. T.; Cras, J. A.; Hummelink, T. W.; Noordik, J. H. *J. Cryst. Mol. Struct.* **1971**, *1*, 253−257. (b) Riekkola, M.-L.; Pakkanen, T.; Niinistö, L. *Acta Chem. Scand. A* **1983**, *37*, 807−816.

(29) (a) Lim, B. S.; Fomitchev, D. V.; Holm, R. H. *Inorg. Chem.* **2001**, *40*, 4257−4262. (b) Ray, K.; Weyhermüller, T.; Neese, F.; Wieghardt, K. *Inorg. Chem.* **2005**, *44*, 5345−5360.

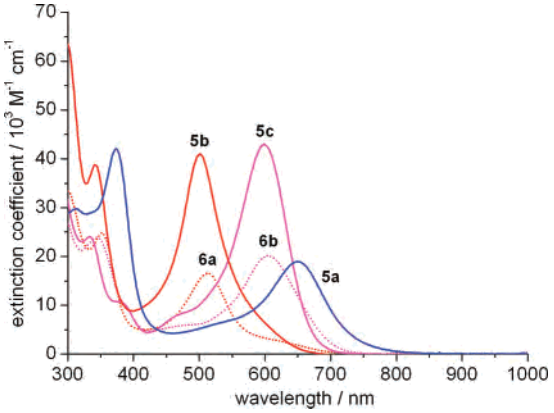

Figure 10. Electronic spectra of **5a** (blue), **5b** (red), **5c** (purple), **6a** (red, dotted), and **6b** (purple, dotted).

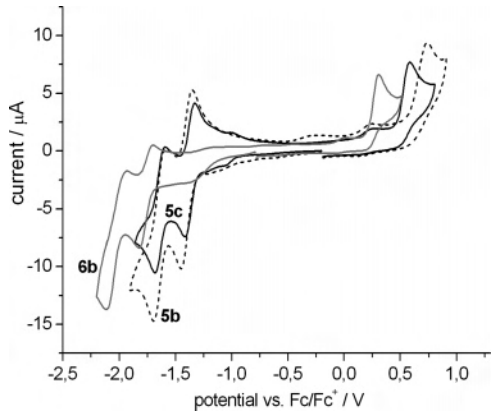

Figure 11. Cyclic voltammograms of **5b** (dotted line), **5c** (black line), and **6b** (gray line) in CH_2Cl_2 (scan rate 100 mV·s^{-1}).

order Ni(II) < Pd(II) < Pt(II).[30] Interestingly, a low-intensity band in the visible part of these spectra with λ_{max} values comparable to those of **5a**/**5b**/**5c** are assigned to a parity-forbidden d−d transition ($^1b_{1g} \leftarrow {}^1a_{1g}$).[31] These absorptions usually follow the energy ordering Ni(II) < Pd(II) < Pt(II) as well, spanning a somewhat larger energy range, as observed for $[\{(EtO)_2PS_2\}_2M]$ (M = Ni, λ_{max} = 689 nm; M = Pd, λ_{max} = 460 nm; and M = Pt, λ_{max} = 420 nm).[30a] In consideration of the high extinction and the marginal influence of the alkyne complex moiety on λ_{max}, the intense low-energy absorptions of **5a**/**5b**/**5c** and **6a**/**6b** are assigned to a MLCT transition between electronic states, which involve predominantly d contributions from the central metal and low-lying carbon sulfur π* orbitals. Actually, the energy ordering of Ni(II) < Pt(II) < Pd(II) has been reported for the complexes $[(C_5H_4CS_2)_2M]^{2-}$, which are likewise furnished with low-lying π* orbitals of a highly π-conjugated ligand.[32]

Cyclic voltammetry displayed two reversible one-electron-transfer waves for **5a**, **5b**, and **5c** (Figure 11). The potentials are nearly independent of the nature of the central metal for both electron transfers, respectively. The potentials of the first transfer ($E_{1/2}$ vs Fc/Fc^+) amount to −1.54 V for **5a**, −1.59 V for **5b**, and −1.56 V for **5c**. In contrast, the substitution of the acetylenedithiolate ligand **3a**$^-$ by **3b**$^-$ results in a distinct change of the redox potential and less-reversible electron-transfer waves. Thus, the potential of the first transfer ($E_{1/2}$ vs Fc/Fc^+) amounts to −1.76 V for **6a**. The isocyanide ligand in **3b**$^-$ renders the Mo−alkyne moiety more electron-rich and harder to reduce. Therefore, both redox processes in **5a**/**5b**/**5c** and **6a**/**6b** are assigned to the alkyne-complex moiety. This conclusion is supported by data of related cationic $[Tp'W(CO)_2(alkyne)]^+$ and neutral $[Tp'W(CO)_2(alkyne)]$ complexes.[25c,8]

This perception is proven by stoichiometric reduction of **5a**/**5b**/**5c** with sodium naphthalide. The one-electron reduction, which is also chemically reversible, affects a shift of both CO stretching frequencies by 30/45 cm^{-1} for **5a** and 35/48 cm^{-1} for **5b**, respectively. Interestingly, the corresponding shift turned out to be smaller for the platinum complex **5c** (10/14 cm^{-1}). The X-band EPR spectra of **5b**$^-$ and **5c**$^-$ in frozen THF solution display rhombic spectra with conspicuously small *g* anisotropy (**5c**$^-$: 2.039, 2.000, and 1.966). Both spectra show high similarity, and the hyperfine coupling is resolved neither to platinum nor to tungsten. The latter observation argues for a high degree of delocalization of the unpaired electron. For comparison, in the mononuclear, paramagnetic complex $[Tp'W(CO)_2(PhC_2Ph)]$, *a*(W) values between 37 and 53 G are observed.[25c] In addition, the EPR signals of related dithiolene complex anions such as $[(Ph_2C_2S_2)_2Pt]^-$ [33] and $[(t\text{-}Bu_2C_6H_2S_2)_2Pt]^-$ [29b] show a much higher *g* anisotropy and *a*(Pt) values about 100 G, indicating a significant metal spin density. Therefore, a contribution of platinum in the LUMO of the complexes **5a**/**5b**/**5c** can be disregarded in accordance with the cyclic voltammetry data. In consideration of the increased π-back-bonding ability of tungsten in the reduced species, the LUMO is assigned to the tungsten alkyne complex entity. Consequently, the dependence of the visible absorption from the central metal is based upon an essential contribution of central metal d orbitals to the occupied frontier orbitals of **5a**/**5b**/**5c**. Thus, the color-determining transition implies partly a metal-to-tungsten charge transfer. This perception corresponds to the results of DFT calculations on **4a**/**4b**.

The observation of only two shifted CO bands seems generally consistent with reduced mixed-valence tungsten centers of class III according to the classification of Robin and Day.[34] The average difference of 250 mV between the first and second electron transfer proves the electronic interaction of both tungsten centers over the central metal ion. This potential difference allows an estimate of the comproportionation constant $K_c > 1.7 \times 10^4$.[35] However, the potential difference is much smaller compared with that of classical dithiolene complexes (ΔE = 900 mV for $[Ni(S_2C_2Me_2)_2]$[29a]), reflecting the larger distance of the redox-active

(30) (a) Jorgensen, C. K. *J. Inorg. Nucl. Chem.* **1962**, *24*, 1571−1585. (b) Isci, H.; Dag, Ö.; Mason, W. R. *Inorg. Chem.* **1993**, *32*, 3909−3914. (c) Cavell, R. G.; Byers, W.; Day, E. D.; Watkins, P. M. *Inorg. Chem.* **1972**, *11*, 1598−1606.
(31) Dingle, R. *Inorg. Chem.* **1971**, *10*, 1141−1144.
(32) Bereman, R. D.; Nalewajek, D. *Inorg. Chem.* **1976**, *15*, 2981−2984.
(33) Bowmaker, G. B.; Boyd, P. D. W.; Campbell, G. K. *Inorg. Chem.* **1983**, *22*, 1208−1213.
(34) (a) Robin, M. B.; Day, P. *Adv. Inorg. Chem. Radiochem.* **1967**, *10*, 247−422. (b) Creutz, C. *Prog. Inorg. Chem.* **1983**, *30*, 11−73.
(35) Richardson, D. E.; Taube, H. *Coord. Chem. Rev.* **1984**, *60*, 107−129.

centers compared with those of dithiolene complexes with high single-electron density at the sulfur atoms. According to the theory of Hush, an intervalence transfer should be observed for the mixed-valence species in the near-IR region.[36] However, while the electronic spectra considerably change by the reduction, no intervalence transfer was detected up to 2200 nm. The intense color-determining transitions of **5a**/**5b**/**5c** are quenched, and the new absorption maxima around 420 nm with lower intensity are typical for absorptions in the alkyne complex moiety (vide infra).

Some further evidence on the electronic structure of metalla-acetylenedithiolate complexes was sought from comparison of the ^{195}Pt NMR shift of **6b** with the corresponding values of related, neutral complexes. Divalent platinum complexes with a S_4 donor set usually display ^{195}Pt shifts in the range of -4000 ± 500 ppm. For [Pt(S_2COEt)$_2$] a value of -4210 ppm[37] and for [Pt{$S_2C_2(CF_3)_2$}$_2$] a value of -3988 ppm[38] have been reported. The platinum center of **6b**, which was detected at -2780 ppm, is remarkably less shielded. This observation can be attributed to a larger paramagnetic deshielding in **6b**. According to the Ramsey equation,[39] a smaller energy difference ΔE of **6b** compared with [Pt(S_2COEt)$_2$] could account for the higher value of the paramagnetic term σ^{para}. If the observed visible transitions are taken as an approximation for ΔE, the absorption of **6b** ($\lambda_{max} = 605$ nm) is consistently lower in energy than that of [Pt(S_2COEt)$_2$] ($\lambda_{max} = 446$ nm). Accordingly, an essential contribution of the central metal ion for the maximum absorption in the electronic spectra of **5a**/**5b**/**5c** and **6a**/**6b** is corroborated by the observation of a strong paramagnetic deshielding effect in the ^{195}Pt NMR of **6b**. However, an interpretation of the shielding effects by simple arguments must be handled with care, because a recent detailed analysis of the chemical shift tensors in [Pt{S_2C_2-$(CF_3)_2$}$_2$] revealed extremely anisotropic shielding effects.[38]

Cluster-Type Complexes with Acetylenedithiolate. Reactions of **3a**$^-$ with Cu(II) precursors led to reduction of copper in all cases. Consistently, treatment of **3a**$^-$ with 1 equiv of [Cu(MeCN)$_4$]BF$_4$ yielded deep red [Cu$_4$(**3a**)$_4$] (**7**). The result of the X-ray diffraction analysis of **7** is depicted together with selected metrical parameters in Figure 12. The most striking feature in this complex is the fact that the tungsten-bound acetylenedithiolate does not coordinate in a chelatelike manner. Four Cu(I) ions form a tetrahedron, and the metalla-acetylenedithiolate ligands bridge its faces. One sulfur atom of an individual acetylenedithiolate coordinates to one copper ion, and the second sulfur atom coordinates to the two remaining Cu(I) ions of the tetrahedral face in a μ^2-like fashion. Consequently, the four thiolate-bridged edges of the copper tetrahedron exhibit short Cu−Cu distances (2.632−2.658 Å) indicating $d^{10}-d^{10}$ center bonding interaction[40] and the remaining two edges are significantly longer (2.787 and 2.880 Å). This structural motif is typical for Cu(I) complexes with monoanionic dithiocarbamates, dithiocarboxylates, and other related sulfur ligands.[41] The bend-back angles in the alkyne complex moiety are distinctively larger in **7** as compared with the chelate complexes **4a**/**4b**, **5a**/**5b**/**5c**, and **6a**/**6b**. The resulting S−S distances of a particular acetylenedithiolate ranging from 3.864 to 3.964 Å are comparable with the corresponding S−S distance in the free anion **3c**$^-$. Remarkably, this angle relief with respect to the corresponding S,S′-chelate complexes leads to shorter alkyne C−C bonds ranging from 3.326 to 3.368 Å. The diameter of the whole cluster amounts to approximately 2 nm.

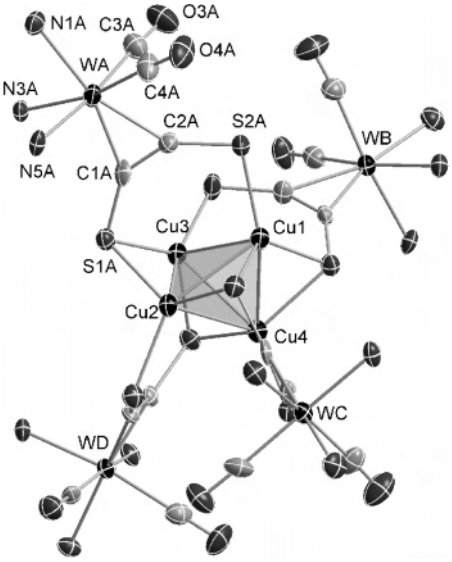

Figure 12. Molecular structure of **7**; Tp′ is omitted except for the N atoms bound to W; 50% ellipsoid probability. Selected bond lengths (Å) and angles (deg), mean values over the four **3a**$^-$ moieties A−D if not noted otherwise: W−C1 2.020(10), W−C2 2.098(9), C1−C2 1.340(13), C1−S1 1.693(10), C2−S2 1.668(10), S1A−Cu2 2.285(3), S1A−Cu3 2.264(3), S2A−Cu1 2.267(3), Cu1−Cu2 2.632(2), Cu1−Cu3 2.880(2), Cu1−Cu4 2.658(2), Cu2−Cu3 2.642(2), Cu2−Cu4 2.787(2), Cu3−Cu4 2.636(2), C1A−C2A−S2A 142.8(8), C2A−C1A−S1A 140.2(8), C1C−C2C−S2C 142.8(8), C2C−C1C−S1C 137.6(8).

The larger bend-back angles and the corresponding changes in the electronic structure of the alkyne complex moiety are reflected in the spectroscopic properties. The alkyne carbon resonances in the ^{13}C NMR spectrum appear remarkably high-field shifted at 257 and 230 ppm (compare free **3a**$^-$, 291 and 252 ppm, and its chelate complex **4a**, 278 and 259 ppm). Two high-intensity absorptions at 513 and 406 nm are found in the visible electronic spectrum of **7**, while free **3a**$^-$ displays only a single absorption of comparable intensity at a mean value of 446 nm (Figure 13, the

(36) Hush, N. S. *Coord. Chem. Rev.* **1985**, *64*, 135−157.
(37) Colton, R.; Tedesco, V. *Inorg. Chem.* **1991**, *30*, 2451−2452.
(38) Kogut, E.; Tang, J. A.; Lough, A. J.; Widdifield, C. M.; Schurko, R. W.; Fekl, U. *Inorg. Chem.* **2006**, *45*, 8850−8852.
(39) Webb, G. A. In *NMR and the Periodic Table*; Harris, R. K., Mann, B. E., Eds.; Academic Press: London, 1978; p 50.
(40) (a) Merz, K. M., Jr.; Hoffmann, R. *Inorg. Chem.* **1988**, *27*, 2120−2127. (b) Pyykkö, P. *Chem. Rev.* **1997**, *97*, 597−636.
(41) (a) Lawton, S. L.; Rohrbaugh, W. J.; Kokotailo, G. T. *Inorg. Chem.* **1972**, *11*, 612−618. (b) Manotti Lanfredi, A. M.; Tiripicchio, A.; Marsich, N.; Camus, A. *Inorg. Chim. Acta* **1988**, *142*, 269−275. (c) Shuerman, J. A.; Fronczek, F. R.; Selbin, J. *Inorg. Chim. Acta* **1988**, *148*, 177−183. (d) Camus, A.; Marsich, N.; Manotti Lanfredi, A. M.; Ugozzoli, F. *Inorg. Chim. Acta* **1989**, *161*, 87−96. (e) Wycliff, C.; Bharathi, D. S.; Samuelson, A. G.; Nethaji, M. *Polyhedron* **1999**, *18*, 949−958.

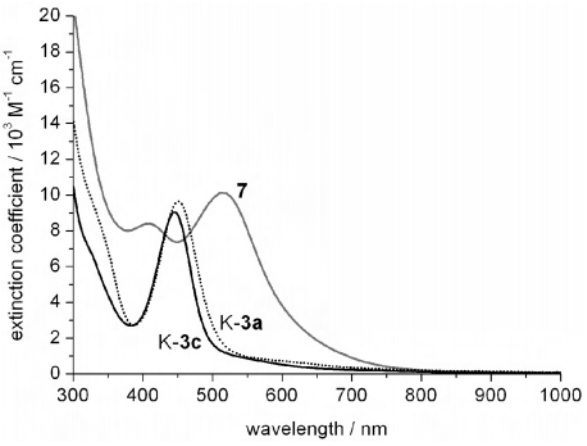

Figure 13. UV−vis spectra of **7** (gray line), K-**3a** (dotted line) and K-**3c** (black line).

spectra of K-**3c** is also given for comparison because ϵ is determined with higher accuracy). This single absorption in **3a**$^-$ is assigned to the HOMO−LUMO transition of the alkyne complex unit. Accordingly, the two absorptions of **7** can be rationalized by a simple MO scheme solely considering the donor interaction of the HOMO of **3a**$^-$ with the p orbitals of copper.

Conclusion

In this contribution, we have described the synthesis and comprehensive characterization of the η^2-*C*,*C*′-acetylenedithiolate complexes K[Tp′(CO)(L)M(η^2-C_2S_2)] (M = W, L = CO, M = Mo, L = CN-*t*-Bu, $CNC_6H_3Me_2$) and its sulfur coordination compounds with [(η^5-C_5H_5)Ru(L)] (L = PPh_3, $CNC_6H_3Me_2$), Ni(II), Pd (II), Pt(II), and Cu(I). Comparison of the molecular structures determined by X-ray crystallography shows that the chelatelike coordination mode of both sulfur atoms of an individual acetylenedithiolate is based on pronounced bend-back angle flexibility. Thus, [Tp′(CO)$_2$W(η^2-C_2S_2)]$^-$ is capable of forming both square-planar biscomplexes with d^8 metal ions and cluster-type complexes, in which acetylenedithiolate bridges two d^{10} ions. The coordination behavior with copper and the M−S bond length in general reveal similar donor strength of our metallaacetylenedithiolate ligands with monoanionic dithiocarbamates. The strong electronic cooperation of metal ions bridged by acetylenedithiolate is reflected in its vibrational, electronic, and EPR spectra and in the electrochemical data, as well. Thus, the CO vibrations at the alkyne complex are generally sensitive to changes in the coordination sphere of the sulfur-coordinated metals. All the S,S′-chelate complexes described in this contribution exist in two oxidation states, which is reminiscent of dithiolene complexes. However, in contrast to dithiolene complexes with a carbon-based backbone, spectroscopic evidence suggests that the redox activity is primarily centered at the metal ions while acetylenedithiolate serves as a very good connector. DFT calculations on dinuclear tungsten ruthenium complexes underline, in very good agreement with the experimental results, that the frontier orbitals are highly delocalized over both metals. According to these calculations, the intense transitions observed in the electronic spectra are attributed to states, which have metal/metal and ligand/metal character. The combination of sulfur donors and the conjugation of these donors with an alkyne-bound metal center in the alkyne complexes of acetylenedithiolate render the resulting dithiolate ligands highly polarizable and soft.

Acknowledgment. The Deutsche Forschungsgemeinschaft is gratefully acknowledged for financial support of this work. We thank Dr. E. Bill (MPI Mülheim) for the EPR measurements. W.W.S. thanks Prof. F. E. Hahn for generous support.

Supporting Information Available: X-ray crystallographic files in CIF format for complexes K-**3c**, **4b**, **6a**, **6b**, and **7**; representation of [K-**3c**]$_4$ in the crystal; metric parameters of geometry-optimized structures of **4a**, **4b**, [Tp(CO)$_2$W(C_2S_2)Ru(C_5H_5)(PMe_3)], and [Tp(CO)$_2$W(C_2S_2)Ru(C_5H_5)(CNPh)]; spin density calculated for **4b**$^+$; UV−vis spectroscopic data of **4a**/**4a**$^+$, **4b**/**4b**$^+$, **5a**, **5b**, **5c**, **6a**, and **6b**; VIS/NIR absorption spectrum of Na[**5b**]; EPR spectra of Na[**5b**] and Na[**5c**] and simulation parameters. This material is available free of charge via the Internet at http://pubs.acs.org.

IC7008286